The Role of Giant Planets in Terrestrial Planet Formation

Harold F. Levison[1]

and

Craig Agnor[2]

Space Studies Department

Southwest Research Institute, Boulder, CO 80302

In *Astronomical Journal*

[1] On sabbatical at: Observatoire de la Cote d'Azur, B.P. 4229, 06304 Nice Cedex 4, France.

[2] Current address: Earth Sciences Department, UCSC, 1156 High Street, Santa Cruz, CA 95064, USA.

Abstract

We present the results of simulations of the late stages of terrestrial planet formation under the gravitational influence of 6 different outer giant planetary systems with a wide range of dynamical characteristics. Our goal is to determine the role that the giant planets play in determining the number, mass and orbital characteristics of the resulting terrestrial planets and their general potential for habitability. Each of the giant planet systems affects the embryos in its own unique way. However, we find that the most profound effects are secular in nature. We also discovered that dynamical excitation of the embryos by the giant planets in one region can be transferred into another on short timescales via what we call *secular conduction*. Despite large differences in the behaviors of our systems, we have found general trends that seem to apply. The number, mass, and the location of the terrestrial planets are directly related to the amount of dynamical excitation experienced by the planetary embryos near $1\,AU$. In general, if the embryos' eccentricities are large each is crossing the orbits of a larger fraction of its cohorts, which leads to a fewer number of more massive planets. In addition, embryos tend to collide with objects near their periastron. Thus, in systems where the embryos' eccentricities are large, planets tend to form close to the central star.

Keywords: solar system: formation — planets and satellites: formation

I. Introduction

Within the last decade, the study of extra-solar planetary systems has moved from the realm of science fiction to the realm of science fact. Radial velocity surveys have discovered, and are continuing to discover, dozens of planets in orbits about stars other than the Sun (see Butler et al. 2002 and Marcy, Mayor & Cochran 2000 for reviews). Although currently limited to gas giant planets, technologies are in development that may soon allow for the discovery and study of Earth-like bodies (some examples are *Kepler*, and *Terrestrial Planet Finder* or *TPF*). Thus, we believe that the time is ripe for studies of the formation of terrestrial planets in extra-solar planetary systems. Our aim is not only to predict and understand what may be found by these programs, but to perhaps aid in the selection of target stars.

The nearly circular, coplanar orbits of the planets in our Solar System strongly suggest that planetary formation occurred in a disk revolving about a star. Following the collapse of the solar nebula to this disk, the modern paradigm envisages four major phases of terrestrial planet formation (eg. Greenberg et al. 1978; Wetherill & Stewart 1993; Lissauer & Stewart 1993; Weidenschilling & Cuzzi 1993). First, refractory planetesimals formed from the condensed material in the disk. As the planetesimal population developed, the second stage began and planetary embryos formed via the accretion of these planetesimals in a process known as run-away growth. The second phase is thought to continue until the planetary embryos grew large enough to gravitationally perturb one another and excite their eccentricities, e (Kokubo & Ida 1998). During this *oligarchic growth* phase there was a balance between dynamical excitation of the embryos by each other and dynamical damping due a background population of small bodies. However, eventually most of the the small bodies were acreted or removed and the orbits of te embryos began to cross. At this time, according to the standard picture, collisions between the planetary embryos allowed larger objects to form (Wetherill

1986; 1996; Agnor et al. 1999). This process continued until all of the available planetesimals in each region were either accreted into larger objects, or dynamically removed. As a corollary, the resulting configuration of planetary embryos that was achieved from this accumulation epoch must have reached a dynamically stable (or nearly so) configuration.

There are many variables that can help define what a terrestrial planetary system will look like. Some of these include the mass of the star, the mass and radial distribution of the proto-planetary disk, the disk metalicity, the gas disk lifetimes, the giant planets, and stochastic events. Wetherill (1996) performed a preliminary study of these issues. He found that the mass of the terrestrial planets is primarily determined by the surface density of solid material in the proto-planetary disk, while the location of the terrestrial planets is primarily determined by the giant planet system. As we will describe detail below, of the important variables that affect terrestrial planet formation, the role of giant planets is probably the least understood. Thus, we concentrate on this particular issue.

Although limited in some respects, Wetherill (1996) showed that the dynamical structure of the outer giant planets can play an important role in determining the the structure of the terrestrial planet system. In particular, he showed that giant planets control the final masses of planets in the Habitable Zones[1] (hereafter HZs) of stars. Three sets of runs were performed using initial conditions consisting of a few hundred $\sim 10^{26}$ g planetary embryos between 0.5-3.8 AU. In the first, Jupiter was moved to $10\,AU$ and terrestrial planets formed in the HZ that were typically a factor of 2 more massive than the Earth. In the second set of runs, Jupiter was

[1] We follow Kasting et al. (1993), who defines the Habitable Zone as the region around a star in which an Earth-like planet (similar mass and composition) can sustain liquid water on its surface. This zone extends from ~ 0.82 to $1.4\,AU$ around a star like the Sun.

included at its current location. In this case, systems similar to the solar system were formed. In the third set of runs, Jupiter was placed at $3.5\,AU$. In these runs, the terrestrial planets that formed in the HZs were typically 50% of the mass of the Earth. In these systems perturbations from the giant planets resulted in the complete removal of planetary embryos exterior to 1.3 AU, which could imply that the asteroid belt also extended into $1.3\,AU$ in these systems. (The inner edge of the asteroid belt in the solar system is at $\sim 2.1\,AU$.) In addition, it is possible to imagine a system in which the giant planets prevent terrestrial planets from forming at all in the HZ. (Indeed, this appears to be the case for the planetary system around 47 UMa, see below). In this case, there could be an asteroid belt in this region.

The Monte Carlo algorithm used in Wetherill's simulations has been used to make important contributions to the field of planet formation (e.g. Wetherill 1990, 1992, 1994a). However, to economically model the dynamical evolution of a system of embryos it approximates their interactions as uncorrelated two-body scattering events and does not include long-range gravitational forces between bodies. Of particular importance, the Monte Carlo algorithm does not directly include secular effects or the effects of mean motion resonances between the planets, which can be important in planetary systems. Wetherill did attempt to include the important mean motion resonances with Jupiter and the ν_6 secular resonances by employing an empirical approximation of their effects. However, it is not clear if his algorithms were sufficiently accurate and he was unable to include either the more subtle resonant effects of the giant planets, or the long-range effects of the embryos themselves. Fortunately, new and very efficient direct integration methods are now available that can perform this type of simulation without these limitations (Duncan et al. 1998; Chambers 1999; Levison & Duncan 2000).

Another limitation of Wetherill's simulations is that at the time they were performed there was no information on the structure of giant planets in extra-solar

systems. This work predates the discovery of extra-solar planets from radial velocity surveys (see Butler et al. 2002 and Marcy, Mayor & Cochran 2000 for reviews) and modern attempts to model the diversity of possible giant planet systems (Levison et al. 1998). As a result, Wetherill restricted his study to the Solar System's giant planets and moved the position of Jupiter and sometimes Saturn in order to mimic the effects of different giant planet systems.

The only simulations of which we are aware of the formation of terrestrial planets in a extra-solar giant planet system is a recent study of the planetary system around 47 UMa (Laughlin et al. 2002). We currently know of two giant planets in this system: one at ~ 2.1AU with a mass of 2.5 Jupiter-masses (assuming $\sin(i) = 1$) and the other at sim3.7AU with a mass of 0.76 Jupiter-masses. Laughlin et al. (2002) studied the evolution of a series of planetary embryos initially spread from 0.3 to 2.0AU under the gravitational effects of the known giant planets (assuming $\sin(i) = 1$) and found that no accretion occurred beyond ~ 0.7AU from the central star, which includes the star's HZ. These authors therefore concluded that this system is unlikely to contain habitable terrestrial planets. This study supports the basic hypothesis of this paper, that the giant planets in a system play an important role in determining structure of the terrestrial planets in a system.

Given the above discussion, we feel it is appropriate to revisit the issue of the role of giant planets on the formation of terrestrial planets in a systematic (or nearly so) way. In this paper we present the results of a series of dynamical integrations of the final stages of terrestrial planet formation under the gravitational influence of differing giant planet systems. We assume that all the stars are the same mass as the Sun and that the proto-planetary nebula was the same as it is believed to have been in our Solar System (see Wetherill 1996 for a discussion). In §2 we discuss the initial conditions and numerical methods. In §3 we present the results of the simulations. In §4 we summarize and present our conclusions.

II. Numerical Methods and Initial Conditions

In this section we describe the methods used to construct our terrestrial planet systems. The first issue to discuss is which giant planet systems to employ in our simulations. Since the initial survey of Wetherill (1996), dozens of giant planets have been discovered orbiting other stars (see Butler et al. 2002 and Marcy, Mayor & Cochran 2000 for reviews). Although such a discovery was anticipated, the nature of the systems discovered came as a complete surprise. In particular, their orbital characteristics are quite different from what was expected from studying the giant planets in our own Solar System. Semi-major (a) axes have been found as small as 0.038 AU (HD83443; Mayor et al. 2002), eccentricities have been found as large as 0.93 (HD80606; Naef et al. 2001), and some planets have been found locked in mean motion resonances with one another (Gliese 876; Marcy et al. 2001). It should be noted that the current observational selection effects of the radial velocity technique restrict it to discovering Jupiter- or Saturn-mass objects close to their parent stars and that planets have only been found orbiting a few percent of the stars studied. In addition, the sample of known extra-solar planets may be contaminated by face-on binary stars (Stepinski & Black 2000). Therefore, although these startling discoveries have taught us that planetary systems can be very different from the Solar System, the searches for extra-solar planets have yet to reveal anything about what 'typical systems' are like.

In order to better understand the range of dynamically long-lived giant-planet systems, Levison et al. (1998, hereafter LLD98) presented the results of a set of bottom-up numerical simulations designed to generate dynamically plausible giant planet systems from a large number of planetary embryos. These simulations produced systems that are stable for at least for a billion years and which exhibit a wide range of characteristics[2]. Some of these systems are reminiscent of the

[2] It should be noted that LLD98 were forced to employ some methods that were clearly unphysical

outer solar system. The number of planets ranged from one to seven. Many systems contained only Uranus-mass objects. LLD98 constructed systems that were more 'compact' than the outer solar system and systems that were much sparser, with planets on very eccentric orbits[3]. In all 27 different giant planet systems were constructed and studied. A complete list and description can be found at `www.journals.uchicago.edu/AJ/journal/issues/v116n4/980173/980173.appx/index.html`.

We employ the results of some of LLD98's simulations in this work. In particular we chose 6 different giant planet systems for our simulations:

NOPL) No giant planets at all. This is used mainly as a control study. By comparing the results of this study to those with giant planets, we can determine how a giant planet system affects the dynamics of the terrestrial planet embryos.

SS) The giant planets in our Solar System (Jupiter, Saturn, Uranus, and Neptune).

II) LLD98's Run 11_a, which is the most compact system they constructed. This system consists of 5 giant planets. There are 3 very massive planets (totaling 8 times the mass of Jupiter) in the region where Jupiter and Saturn reside in our solar system. It has a 1:2 mean motion resonance between the two innermost planets. The resonance has a small libration amplitude of $\sim 15^\circ$ which implies that the two planets are deeply embedded in this resonance.

III) LLD98's Run 14_a, which has the largest number of giant planets. This system has a total of 7 Neptune-mass planets. It may be indicative of the types of systems that form when the gas part of the proto-planetary nebula disperses before the planets grow large enough to accrete H/He envelopes.

---

and thus their techniques were not the same as those that the universe uses to build giant planets. However, their goal was not to model planetary formation as such, but only to construct a wide range of dynamically plausible synthetic solar systems.

[3] See LLD98 for a precise definition of compactness.

IV) LLD98's Run 4_a. This system contains 3 Saturn-mass planets on orbits that are significantly more eccentric than the giant planet orbits in our Solar System, but are similar to some of the multi-planet extra-solar systems. The two innermost planets in this system are close to, but not in, the 1:2 mean motion resonance.

V) LLD98's Run 12_b. This system consists of a single Jupiter-mass planet on a very eccentric orbit. It has a semi-major axis of 17 AU and an eccentricity of ~ 0.8, which leads to a perihelion distance of 3.7 AU. This system is the result of a global instability of a 7 planet system, where many of the planets had masses similar to Jupiter and Saturn. The time evolution of this system is shown in Figure 3 in LLD98[4].

Diagrams of these systems are presented in Figure 1 and they are described in detail in Table 1. It is important to note that the inclinations reported in the table are with respect to the initial invariable plane (hereafter IIP) of the planetary embryos from which the giant planets form. Since mass and angular momentum was lost during the giant planet formation due to ejections and planets hitting the central stars, the invariable plane of the resulting giant planet system may not be the same as the original. The differences are usually small. However, it should be noted that the sole planet in System V has an inclination of 22°.

Our simulations began with initial conditions that are broadly consistent with the runaway growth of lunar- to Mars-sized planetary embryos and the subsequent

[4] One interesting aspect of this system is that several of the giant planets hit the Sun during the most violent parts of the instability. This could have disrupted the proto-planetary disk in the inner system making terrestrial planet formation impossible. Nonetheless, we adopt this system for completeness since it could be possible for such a system to have formed without disrupting terrestrial planet region.

sweep up of smaller planetesimals. These processes could have occurred in as little as $\sim 10^5$ (e.g. Wetherill & Stewart 1993) and $\sim 10^6$ years (Weidenschilling et al. 1997) respectively. Since we are primarily concerned with the effect of gravitational perturbations from the giant planets on the formation of the terrestrial planets, we have excluded any interactions that may have competed with velocity excitation from the outer planets (e.g. dynamical friction with a swarm of smaller planetesimals (Wetherill and Stewart 1993), and/or eccentricity damping via density wave torques in a remnant of the gas disk (Agnor & Ward 2002)). Accretion models using similar simplifications have been generally successful at describing the formation of the terrestrial planets in our own solar system (e.g. Wetherill 1990, Agnor et al. 1999, Chambers 2001).

We started our simulations with 100, $m = 0.04 M_\oplus$ planetary embryos between 0.5 and 3.0 AU. These embryos were distributed such that their surface density varied as $r^{-3/2}$ and had a value of 8.0 g/cm^2 at 1 AU. This results in an initial spacing of the embryos in semi-major axes (a) that was roughly $5 r_H$, where $r_H = a\,(M/3M_\odot)^{1/3}$. Our initial conditions are comparable to minimum mass nebular models with $2\,M_\oplus$ interior to 1.5 AU (see e.g. Weidenschilling 1977). Our choice of the inner edge of the proto-planetary disk was dictated by practical considerations because this choice determines the timestep of the simulations and thus the amount of CPU time required. Each embryo had a density of $3\,\mathrm{g/cm^3}$. We randomly chose the initial Hill eccentricity, e_H, of an embryo from a uniform distribution between 0.5 and 5, where $e_H = e \times (a/r_H)$. The initial inclination of each embryo was set to half its initial eccentricity. Since we intended for the terrestrial planets to be built from the same disk that formed the giant planets, we took these inclinations to be with respect to the IIP. An embryo's mean anomaly, periapse, and ascending node were selected randomly. We performed 4 simulations in each of the giant planet systems in Table 1. Each of these had identical initial

conditions except for a different random number seed. An example of the initial conditions for the embryos in one of our runs is shown in Figure 2.

The orbits of the embryos and giant planets were integrated using a full N-body, symplectic algorithm known as SyMBA (Duncan et al. 1998) modified to handle small perihelion passages (Levison & Duncan 2000). This code has the speed of the highly efficient computer algorithm developed by Wisdom & Holman (1991), but in addition it can accurately handle close encounters between objects. We employed a timestep of 0.015 yr and, unless otherwise noted, the simulations were integrated for a total of 2×10^8 years. The simulations were performed in a gas-free environment.

The fact that for large numbers of bodies the computational cost of our calculation scales as N^2 (where N is the number of bodies followed), places a practical constraint on the number of bodies which can be used. For this reason, we did not include any residual population of smaller planetesimals left over from the runaway and post-runaway stages of embryo growth in our simulations. Also, collisional fragmentation of embryos was not included, since any process which would tend to increase the number of bodies in a simulation is not computationally feasible. In these simulations, when two embryos collided they were merged inelastically. The radius of the new body was computed by adding the volumes of the colliding bodies and assuming uniform density and spherical shape for the new combined body. The orbit of the new body was calculated assuming conservation of momentum.

III. Results

The analysis of our simulations proceeds as follow. In §3.1 we describe the final terrestrial planet systems, while concentrating on the systematic variations found in the different giant planet systems. In §3.2 we investigate the differences in the dynamics of the embryos that lead to these systematic variations. Finally, in §3.3 we describe the different dynamical mechanisms through which the giant planet systems affect the orbital evolution of embryos.

3.1 The final terrestrial planet systems

As we mentioned above, we constructed 4 terrestrial planet systems in each of the giant planet configurations described in Figure 1 and Table 1. Our final synthetic terrestrial planet systems are compared to the real terrestrial planets in Figure 3. In these figures the positions of a circle along the abscissa indicates the planet's semi-major axis. The size of the circle indicates the planetary mass. In addition, the mass of the planet, in Earth masses, is printed above each planet. The markings beneath each planet indicate the range of distances from the planet's central star (periastron and apastron) with the central vertical line indicating the semi-major axis.

Figure 3B shows the systems that form when there were no giant planets. Note that in these systems accretion is not yet complete after 2×10^8 yr as indicated by objects on crossing orbits. Indeed, this figure is somewhat misleading since only those planets with semi-major axes less than 2.5 AU are plotted. At 2×10^8 years, these systems still contain between 23 and 29 objects. Thus as an illustration, in Figure 4 we plot the semi-major axis and eccentricity of all the bodies in the upper system in Figure 3B. Although this system contains 24 objects at 2×10^8 years (top of Figure 4), the planets inside of ~ 2 AU are almost fully formed. The small bodies that remain are external to the large terrestrial planets and were scattered out to

their current orbits by their larger siblings. This is true for all 4 of the systems in Figure 3B.

In order to determine the fate of the small objects beyond 2 AU, we extended the integration of the system in Figure 4 to a billion years. The resulting system is shown in the bottom panel of the figure. We see that the disk of small objects continues to spread to larger semi-major axes. A $\frac{1}{2}M_{\oplus}$ planet formed at ~ 4.3 AU. This is well beyond the outer edge of the original proto-planetary disk and thus is a result of collisions that occurred between objects that formed closer to the star. In addition, the large planets within 2 AU are still accreting — for example, the $0.8\,M_{\oplus}$ planet accreted a small object at 875 Myr. Indeed, most likely all the small objects in all these systems will be accreted before they are ejected, but this process could take tens of billions of years (Tremaine 1990).

Figure 3C shows the results of the four simulations done under the influence of the giant planets in the Solar System. Since this problem has been studied in great detail by other authors (Wetherill 1986; 1994b; Chambers & Wetherill 1998; Agnor et al. 1999 Chambers 2000; 2001), we only briefly discuss it. These simulations can can be compared with Figure 3A which shows the real terrestrial planets in the same manner. The agreement is quite good. Our simulations usually produce 2 large terrestrial planets with masses and locations similar to Earth and Venus. However, planets near 1.5 AU tend to be more massive than Mars and the eccentricities of the larger planets ($\sim 1M_{\oplus}$) are larger than those observed for Earth and Venus. This result is consistent with previous attempts at the same problem (Chambers & Wetherill 1998; Agnor et al. 1999). It is not clear why these differences occur and thus this is an area of active research (for example see Agnor & Ward 2002).

Comparison between these systems and those that formed in the absence of giant planets (Figure 3B) show important similarities and important differences. Unlike the systems in Figure 3B, those that formed in the presence of the giant

planets do not have large planets beyond roughly 1.5 AU. However, interior to $\sim$ 1.5 AU the mass, semi-major axes, and eccentricities of the terrestrial planets are remarkably similar. This implies, and we argue this in more detail below, that the giant planets in the Solar System did not play an important role in the terrestrial formation process interior to Mars's orbit.

The terrestrial planets that formed under the influence of the giant planet system II (Figure 3D) show two distinct differences from those in Figure 3C. First, there are no large terrestrial planets outside of 1 AU. Second, the largest terrestrial planets in these runs are typically more massive than those that formed under the influence of giant planets in the Solar System.

The terrestrial planet systems that formed under the influence of the giant planet system III with 7 small giant planets (Figure 3E) are remarkably similar to those that formed under the Solar System's giant planets. The only significant difference is that planets interior to 1 AU are slightly larger. One the other hand, the results of the simulations done under the influence of the giant planet system with 3 eccentric Saturn-mass giant planets (System IV) are remarkably different from those that formed in the other outer planetary systems so far discussed in that no large planet forms outside of $\sim$ 0.8 AU (Figure 3F). Finally, the system with one large very eccentric giant planet (System V) produced terrestrial planets that are the most different from those in Figure 3C. These systems tend to have smaller planets close to the star (Figure 3G).

Although the above results clearly show that the giant planet system can play an important role in determine the size and location of the terrestrial planets, it is interesting to note that 'habitable' planets formed in each of our giant planet systems. Here we are defining a 'habitable' planet as one that lies in the HZ of a star (Kasting et al. 1993, see above) and is large enough to be able to support

an Earth-like environment[5]. Williams et al. (1997) suggest that the most severe constraint on habitability is the planet's ability to support a carbonate-silicate cycle that serves to regulate the CO_2 levels in the atmosphere. This cycle requires plate tectonics, or simular process, which removes CO_2 from carbonate sediments and returns it to the atmosphere. Williams et al. (1997) argue that a planet's mass must be $\gtrsim 0.23\,M_\oplus$ for its surface to volume ratio to be small enough so that radiogenic heating can support plate tectonics.

Every one of our giant planet systems produced at least one planet in the HZ more massive than $\sim 0.23\,M_\oplus$. However, not all runs did so. The runs with no giant planets always produced a planet this massive in the HZ. The System SS runs produced such a planet in 3 out of 4 simulations. Indeed, in the last run, a $1.2\,M_\oplus$ planet formed with $a = 1.41$ AU, which is just outside the HZ. System III produced a $M \gtrsim 0.23\,M_\oplus$ planet in the HZ in half of the simulations. Finally, the remaining giant planet systems produced such a planet in one quarter of the simulations.

Therefore, the architecture of the giant planets can significantly affect the chances of finding a large planet in the HZ. This result can be used to help develop a target list for spacecraft like the TPF. Giant planets are usually much easier to detect than Earth-mass objects. Since the structure of the giant planet systems can be used to constrain the existence of habitable terrestrial planets, it may be more efficient to search for the giant planets in a system before expending the resources to search for the terrestrial planets.

With this in mind, we examine our simulation results and attempt to identify systematic differences between the terrestrial planets in different giant planet systems we investigated (which hopefully can be applied to other systems as well).

---

[5] Certainly, there are other environmental issues that affect habitability, for example sources of volatiles and impact rates. This issue will be addressed in future papers.

We find two major systematic differences: 1) the masses of the largest planets, and 2) the location of the planets. It is possible to quantify these differences. We have found that the best measure of location is the mass weighted semi-major axis of the terrestrial planets ($\langle a \rangle$) [6], while the best measure of mass is the mass of the largest planet (M_{max}). Thus in Figure 5 we plot the ranges of these values for each set of runs in the various giant planet systems.

We start our interpretation of Figure 5 by noting a significant correlation between M_{max} and $\langle a \rangle$ for those systems with $\langle a \rangle \gtrsim 0.6\,\mathrm{AU}$. The most natural explanation for this correlation is that the giant planets are somehow transporting proto-planetary disk material inward which increases the amount of material close to the star, allowing larger planets to form. We describe the physical mechanisms that control this behavior in the next subsection.

The fact that the two systems with $\langle a \rangle \lesssim 0.6\,\mathrm{AU}$ have smaller M_{max} than predicted from an extrapolation of the above correlation is the result of impacts with the star. For example, an average of 16% of the embryos in the System SS runs hit the central star (which we set to the radius of the Sun), while this value is 46% and 68% for the System IV and System V runs, respectively. These two systems are clearly more effective at moving material inward than the other giant planet systems. We note that massive terrestrial planets do not form inside of 0.5 AU. The most likely explanation is that this is a result of our placement of the inner edge of the initial proto-planetary disk at 0.5 AU. In these cases, material delivered to regions interior to 0.5 AU find that there is nothing to collide with. Rather than forming a planet, the material is driven into the star. Thus, we believe that if we

[6] This is calculated using only those objects that are not on giant planet-crossing orbits and those objects that have suffered at least two mergers. The latter constraint was added to remove the low mass, objects scattered outward in the NOPL runs.

had disks that extended inward of 0.5 AU, we would most likely be forming massive terrestrial planets in these regions in the System IV and System V runs.

However, even if the disk extended all the way to the star, we would not expect the trend of increasing M_{max} with decreasing $\langle a \rangle$ to also extend all the way in for two reasons. First, it is easier to drive embryos with small semi-major axes into the star than ones with large semi-major axes and so regions of the disk close to the star will still become depleted of material. Second, collisional fragmentation will most likely be more severe close to the star because of higher orbital velocities (Wetherill 1988) and thus more mass will be lost to collisional cascade.

3.2 The role of dynamical excitation in terrestrial planet formation

The correlation between M_{max} and $\langle a \rangle$ seen in Figure 5 is the primary result of this investigation and is a prediction of what we expect to see in extra-solar terrestrial planetary systems. In this subsection, we investigate the mechanisms that create this relationship. Since the embryos that form the terrestrial planets only interact with the giant planets through long-range gravitational forces, it is most natural to first investigate the initial dynamical evolution of the embryos in the different giant planet systems.

As a measure of the dynamical excitation of the embryos in a system, we use the mass-weighted RMS eccentricity of all embryos with $0.9 < a < 1.5$ AU, $e^\star$, calculated 10^7 years into the simulation[7]. We chose this range of semi-major axis because this is the region where we see the largest systematic difference in the final masses and locations of the terrestrial planets and because it is near the HZ.

[7] A note on notation. $e^\star$ is specifically defined to be the RMS eccentricity between 0.9 and 1.5 AU. We use $\langle e^2 \rangle$ and e_{RMS} to refer to the mean square eccentricity and root mean square eccentricity, respectively, at arbitrary locations.

Hereafter, we refer to the $0.9 < a < 1.5$ AU region as the *study zone* or SZ. We chose 10^7 years as our standard time because it is long compared to the important secular periods in the giant planet systems, so the giant planets have time to affect the embryos, and yet it is short compared to the amount of time its takes a significant terretrial planet to grow and start to dominate the embryos' dynamics.

Each symbol in Figure 6 shows the range of $\langle a \rangle$ and $e^\star(10^7)$ for the runs from one of our giant planet systems. There is a strong correlation between the dynamical excitation in the SZ and the mass of the largest terrestrial planet. Combining this result with the results in Figure 5, we find an additional correlation between M_{max} and $e^\star$. We interpret these relationships as indicating that the dynamical excitation of embryos near $1AU$ results in the inward transport of material and thus larger planets closer to the star.

Here is how the process works. As the eccentricities of the embryos increase, their radial excursions also increase. That is, they travel over a larger fraction of the disk. As a result, the number of potential merger partners also increases. This can be seen in the top two panels of Figure 7 which shows the semi-major axes and eccentricity of embryos from a run in System NOPL on the left and System II on the right. In these panels, the horizontal bars mark the range of radial excursions for each of the embryos. Notice that the embryos in the System II run are more excited (i.e. have higher eccentricities) than those in the System NOPL run and thus have larger radial excursions.

How is accretion in our simulations influenced by these large eccentricities? To address this issue, the bottom two panels in Figure 7 show the probability per year that a target body in each simulation will collide with each of its neighbors. The impact probability rates were calculated using the method of Bottke et al. (1994), which is based on the formalism of Öpik (1951) and can handle eccentric targets. The characteristics of the target were determined by taking the average of all

embryos in the SZ. For the simulation in System NOPL, the eccentricity of the target is 0.15, while it is 0.24 in the System II run.

In both simulations, the target bodies are roughly 10 times more likely to collide with an object at its periastron than one at its apastron. This is simply a result of geometry. When two objects are at the same distance from the star, r, (so they can collide) their impact probability is proportional to the ratio of their mutual collisional cross-section to the surface area of a sphere of radius r. Thus, in the regime where gravitational focusing is not important (which is true here) and embryos are approximately the same size everywhere, the impact probability should $\propto r^{-2}$, which is roughly what we observe in Figure 7.

We can now put all of our results together to explain the correlation in Figure 5. Different giant planet systems dynamically excite the eccentricities of the terrestrial embryos by differing amounts. Embryos in systems with large eccentricities are on orbits that cross a larger fraction of their peers than in systems with small eccentricities. The large eccentricities make it difficult for the growing planets to become isolated from one another, which leads to fewer and more massive terrestrial planets[8]. This relationship is true unless the giant planets can drive embryos into the central star (as with Systems IV and V). However, once excited an embryo is much more likely to collide with an object near its periastron distance than elsewhere in its orbit. So, if the system of embryos is excited, planets are more likely to form near the inner edge of the disk. Putting the arguments together, in systems where the giant planets can significantly excite the embryos, we tend to build more massive planets closer to the center star.

---

[8] Recall that we do not include fragmentation in our simulations. Fragmentation could somewhat inhibit planetary growth in dynamically excited systems.

3.3 Excitation Mechanisms

In the last subsection we demonstrated how dynamical excitation of the terrestrial embryos by the giant planets (as measured by the value of $e^\star$ at 10^7 years) can lead to changes in the location and masses of the final terrestrial planets. We now investigate the various dynamical mechanisms employed by the giant planets to excite the embryos. Again, for the reasons discussed above, we concentrate on the SZ region.

Figure 8 shows the average $e^\star$ for our runs in each of our giant planet systems. To generate each panel, we first plotted the run with no giant planets (NOPL) in orange and then superimposed the run of the giant planet system of interest (marked in the upper left) in black. As a result, is it trivial to observe the differences that the inclusion of the the giant planets has on the behavior of each system. In order to minimize small number statistics, we took the average of all 4 runs in each giant planet system to generate each curve.

Before we discuss the systems with giant planets, it is useful to understand the behavior of the NOPL system. The initial conditions for the embryos were such that they crossed each other's orbits. As a result, the initial evolution of the system is dominated by close encounters between the embryos. Figure 8A shows a logarithmic growth in $e^\star$. This is caused by gravitational interactions of the embryos which spread the disk and increase eccentricities.

We analytically estimate the growth rate of the mean square eccentricity ($\langle e^2 \rangle$) using the the results of Stewart & Ida (2000). Scattering events redirect the velocity of an embryo converting orbital motion into random motion. The general effect is to excite the orbital eccentricities of the embryos. The excitation rate of the mean square eccentricity due to self-stirring of the swarm is

$$\frac{d\langle e^2 \rangle}{dt} = \frac{n}{\pi^{1/2}} \left(\frac{\sigma a^2}{M_\odot} \right) \frac{M}{M_\odot} \frac{BJ_e}{\langle e^2 \rangle}, \qquad (1)$$

where J_e is an integral function of the ratio between the inclinations and eccentricities, n is the mean motion, σ is the surface density of embryos and B is a logarithmic function of the embryo masses (M) and eccentricities (Stewart and Ida 2000). For the systems of embryos considered here these functions are effectively constants taking the values $J_e \approx 2$, $B \approx 25$. Expressing this rate as an eccentricity growth timescale due to close encounters yields

$$\tau_e = \frac{\langle e^2 \rangle}{\frac{d\langle e^2 \rangle}{dt}} \approx \frac{\pi^{1/2}}{50} \left(\frac{M_\odot}{\sigma a^2} \right) \left(\frac{M_\odot}{M} \right) \frac{\langle e^2 \rangle^2}{n}. \tag{2}$$

Using in the appropriate values for the our simulations, we find that $\tau_e \approx 3.4 \times 10^{10} \langle e^2 \rangle^2$ yrs. This predicts that 10^6 years are required for the eccentricity to grow to $\langle e^2 \rangle^{1/2} = 0.07$, which is what we observe in Figure 8A.

At some point in the evolution an equilibrium is reached when the excitation of the embryos due to mutual scattering is balanced by damping due to physical collisions between embryos (Ward 1993). For a unimodal mass distribution the equilibrium $e^\star$ is

$$e^\star_{\rm equil} \approx 1.8 \left(\frac{m}{M_\odot} \right)^{\frac{1}{3}} \left(\frac{\rho_b a^3}{M_\odot} \right)^{\frac{1}{6}}, \tag{3}$$

where m is the mass of the embryos and ρ_b is their bulk density. For our system, this equation predicts $e^\star_{\rm equil} \approx 0.13$. Figure 8A confirms this prediction. The system reaches its steady state at 5×10^6 years and remains there until 1.7×10^8 years. The drop in $e^\star$ after this time is due to the formation of a large ($\sim 0.5 M_\oplus$) embryos in the SZ which subsequently undergoes a decrease in eccentricity due to dynamical friction with it smaller neighbors. The value of $e^\star$ decreases because we calculate it using a mass-weighted average.

We now address the dynamical mechanisms by which the giant planets excite the embryos in the SZ. We will concentrate on explaining the differences seen in Figure 8 and address each dynamical mechanism in turn.

Forced secular motion by the inner giant planet: A massless body that is under the gravitational influence of a giant planet will undergo oscillations in eccentricity with an amplitude that is on the order of the eccentricity of the giant planet and a period that is on the order of its precession period. For example, employing a standard secular model (see e.g. Brouwer & Clemence 1964) and assuming that the initial eccentricity of the test particle is zero, the maximum eccentricity that it can obtain is

$$e_{max} = 2e_p \frac{b_{3/2}^{(1)}(\alpha)}{b_{3/2}^{(2)}(\alpha)}, \tag{4}$$

where e_p is the eccentricity of the giant planet, α is the ratio of the particle's semi-major axis (a) to that of the planet (a_p), and $b_s^{(m)}$ are Laplace coefficients. Note that the maximum eccentricity is a function of semi-major axes.

The time it takes to reach the maximum eccentricity is $2\pi/g$, where g is the particle's precession frequency. The same theory used to calculate e_{max} gives

$$g = \frac{1}{4} \frac{M_p}{M_\odot} \alpha^2 \, n \, b_{3/2}^{(1)}(\alpha), \tag{5}$$

where M_p is the mass of the planet and n is the mean motion of the particle, and $a_p > a$.

We find that this mechanism is important in two of our giant planet systems (III & V). Figure 8D shows a distinct difference between the runs of System III and those in NOPL at times between $\sim 10^5$ and $\sim 5 \times 10^6$ years, with a peak at roughly 2×10^6. For this system Equation (5) predicts that a particle in the middle of the SZ should have $g = 2.5 \times 10^{-6}$, which implies that particles should reach their maximum eccentricity at 2.5×10^6 years. Equation (4) predicts a maximum eccentricity of 0.11. These two values are consistent with the differences between this System and NOPL. Indeed, Figure 9A shows the averaged $e^\star$ for the runs in this System (red curve) (which is simply a reproduction of the black curve in Figure 8D). The green curve shows the behavior of a massless test particle initially

on a circular orbit as predicted by the theory of forced secular motion. There is general agreement between the behavior of the embryos in the simulations (red curve) and that predicted by the secular theory (green curve).

Perhaps more impressive is the behavior of the embryos under the gravitational influence of System V. Figure 8E shows that the embryos reach eccentricity ~ 0.3 in only a million years! Recall that System V consists of a single Jupiter-mass planet on an orbit with a semi-major axis of 17 AU and an eccentricity of ~ 0.8. The large planet coupled with a very large eccentricity leads to very strong forcing of the embryos. Figure 9B again shows the behavior of the embryos in this system (red curve) and that of the massless test particle (green curve). However, the trajectory of the test particle in this case was determined by direct numerical integrations since the linear theory described above is no longer valid for planets with such a large eccentricity.

So, we have found that the forced secular motion caused by the inner giant planet can play an important role in the dynamics of embryos in our systems. Indeed, if the mass and eccentricities of the innermost giant planet are large enough (as in systems III and V) secular forcing can be the dominant excitation mechanism for planetary embryos in the study zone. In the case of System V, secular forcing was strong enough to throw 68% of the embryos into the central star, reducing the efficiency of planet formation and leading to the accretion of only smaller terrestrial planets close to the inner edge of the embryo disk.

There is one issue that should be discussed before moving on. When attempting to interpret how orbital dynamics influence accretion, it is quite often assumed that large eccentricities correspond to large relative (or random) velocities between the embryos. Relative velocities are important because they effect gravitational focusing and thus the timescale for accretion. For orbits that are randomly oriented (i.e.

uniformly distributed in and longitude of periapse, ϖ and ascending node, Ω),

$$v_x = v_c \sqrt{\frac{5}{8}\langle e^2 \rangle + \frac{1}{2}\langle i^2 \rangle},$$

where v_x is the random or relative velocity (Lissauer & Stewart 1993) and v_c is the local circular velocity. However, in many of the mechanisms that we discuss in this paper, eccentricities and inclinations are forced in such a way that ϖ and Ω are not random (i.e. the orbits are aligned). Thus, e and i are no longer a good measure of relative velocity[9]. This is particularly true of secular forcing.

To ascertain the importance of this behavior in our simulations we calculate v_x in the following way. At particular times during the simulation, we first search for pairs of objects that are both in the SZ and whose radial excursions overlap (i.e. the region from periapse to apoapse overlap). For each pair, we identify the locations of the crossing points, assuming that the orbits are planer[10]. If the orbits intersect, we calculate the magnitude of the relative velocity at the crossing points. If the orbits do not intersect (i.e. they are aligned) we set the relative velocity of the pair to zero. We then calculate the mean relative velocity of all the pairs. Note that if the orbits are all aligned this value will be zero.

Figure 10 shows a comparison between $e^\star$ (black) and this mean crossing velocity, $\langle v_x \rangle$, (green curve) for one of the runs in System III and one in System V. The vertical axes of the two curves ($e^\star$ left and $\langle v_x \rangle$ right) are scaled so that if

---

[9] This issue was studied in detail for small planetesimals in a dense solar nebula by Kortenkamp & Wetherill (2000). They found an enhancement in the accretion rate over what would be expected for the observed eccentricities and inclinations due to the alignment of orbits.

[10] This assumption is required to insure that the orbits cross if they are not aligned. Thus the results of this calculation should be taken as approximate, but are probably good to better than 10%.

the orbits are randomly oriented the curves will overlap. We accomplished this by scaling the crossing velocity by $\sqrt{2}v_c$, where v_c is the circular velocity in the middle of the SZ and the $\sqrt{2}$ is to account for the fact that we are averaging over the magnitude of a 2-dimensional vector.

For both runs shown in Figure 10, we can easily see the role of orbit alignment at early times. On timescales less than a few million years, the relative velocity of the embryos is significantly smaller than their eccentricities would predict. This can have profound effects on the accretion rate of the embryos. This is because the collisional cross-section, σ, is a strong function of v_x, i.e. $\sigma = \pi R^2 \left(1 + v_{esc}^2/v_x^2\right)$, where R is the physical radius of the embryo, the term between the parentheses is the so-called gravitational focusing factor, and v_{esc} is the escape velocity between of the embryos. For example, in our System V runs, there are 15 embryo mergers between 2×10^5 years and 4×10^5 while the orbits are aligned, but only 6 between 5×10^5 and 7×10^5. This is true even though the number of embryos only decreases by $\sim 10\%$ over the same time period. Thus, terrestrial planet accretion will not necessarily be slowed by large e if encounter velocities remain low due to orbit alignment.

It should be noted that the orbit alignment helps at the beginning of the System V simulation as well. As described above, our simulations are assumed to begin at the end of run-away growth. Thus, we assume that the embryos are fully formed. This process takes about 10^5 years (Wetherill & Stewart 1993). If we were to interpret $e^\star$ as a measure of relative velocity, then we might conclude that the embryos never form in the System V runs because the forced eccentricity is large enough to stifle run-away growth. However, because of orbit alignment, the relative velocities remain small for over 3×10^5 years, (a timescale longer than that required for the run-away growth of our initial embryos.

Thus, we conclude that it important to account for orbit alignment when

considering the planet formation scenarios (see also Kortenkamp & Wetherill 2000). It should be noted, however, that orbit alignment does not appear to play an important role in our other systems where secular forcing is not the primary source of excitation.

Secular Resonances: Secular resonances are commensurabilites between the precession rate of embryos and those of the giant planets. The precession rate of the embryos is determined, for the most part, by the gravitational effects of the giant planets, so embryos further from the star tend to have faster precession rates because they are closer to the giant planets. These commensurabilities facilitate the exchange of orbital angular momentum (but not energy) between the giant planet system and the embryos. This exchange results in large increases in embryo eccentricities and/or inclinations without altering their semi-major axes. Thus, secular resonances can act as a principal dynamical excitation mechanism of planetary embryos near 1 AU. Here we are interested in mechanisms that increase the eccentricity of the embryos. Thus, we will start our analysis with the periapse secular resonances.

In linear secular theory, changes in eccentricity are coupled with the precession of the the longitude of periapse, ϖ (Brouwer & Clemence 1964). The apsidal precession of an N-planet system can be represented by N eigenfrequencies (g_j), where N is the number of planets. In the secular model it is convenient to use the variables $h = e \sin \varpi$ and $k = e \cos \varpi$ and the Laplace-Lagrange equations of motion for a small object interior to the planets can be written as

$$h = \mu \sin (gt + \beta) + \sum_{j=1}^{N} \frac{\mu_j}{g - g_j} \sin (gt + \beta_j) \tag{6}$$

$$k = \mu \cos (gt + \beta) + \sum_{j=1}^{N} \frac{\mu_j}{g - g_j} \cos (gt + \beta_j),$$

where μ and β are derived from the initial conditions, and μ_j and β_j are related to the masses and orbital elements of the giant planets. The particle's precession rate is

$$g = \frac{n}{4} \sum_{j=1}^{N} \frac{M_j}{M_\odot} \left(\frac{a}{a_j} \right)^2 b_{3/2}^{(1)},$$

where n is the mean motion of the particle, and M_j and a_j are the mass and semi-major axis of planet j, respectively (this is just an extension of equation 5 to an N-planet system). Note that g is an increasing function of a. As $g \to g_j$ one of the denominators in the sums in Equation 6 is goes to zero. These are the locations of periapse secular resonances. Since $e = \sqrt{k^2 + h^2}$ the eccentricity can reach large values near the resonances in this theory.

In our Solar System, there are two secular resonances (ν_5 and ν_6) that can significantly affect the behavior of the embryos (recall that the embryos are initially spread between 0.5 and 3 AU). Chambers & Wetherill (1998) noted that these resonances played a role in some of their simulations. The strongest resonance is the ν_6 where $g = g_6$, which is associated with the precession of Saturn's apse. In a system that contains just Jupiter, Saturn, Uranus, Neptune, and test particles on circular, coplanar orbits, particles near 2.1 AU are in the ν_6. However, in our simulations, the embryos are massive. By itself a massive embryo disk would cause embedded embryos to undergo apsidal regression (Ward 1981). In conjunction with the prograde precession due to the outer planets, the disk simply decreases precession frequencies and thus moves secular resonances outward. We have estimated the location of the ν_6, by calculating the precession frequencies of the test particles under the gravitational influence of the giant planets and a smooth disk[11] of $4M_\oplus$ spread from 0.5 to 3 AU. The disk moves the ν_6 to ~ 2.2 AU. The ν_5

[11] This code was kindly supplied to us by Martin Duncan. It calculates the precession rates by numerically taking derivatives of a potential that is generated by $\sim 10^4$ rings. These rings are

resonance, which is a commensurability with the frequency associated with Jupiter, is located at $\sim 0.7\,\mathrm{AU}$ if there is no disk and $\sim 1.1\,\mathrm{AU}$ in the presence of the disk.

As first noted by Chambers & Wetherill (1998), the effects of the ν_6 resonance can clearly be seen in the behavior of the embryos, while the ν_5 is not readily apparent. For example, in Figure 11 we compare the behavior of the embryos in our SS simulations to that of test particles. The orbits of the test particles were integrated under the influence of the 4 giant planets in our Solar System and a $4M_\oplus$ disk with the same surface density distribution as the embryos. The red and green dots show the eccentricity as a function of semi-major axis of the embryos and test particles, respectively, at 10^6 years. The ν_6 at 2.2 AU can clearly be seen driving objects into the central star ($e \rightarrow 1$) in both datasets.

The influence of the ν_5 resonance is a bit more subtle, if it is important at all. With the location of this resonance at 1.1 AU, we might expect that it would also strongly influence embryo dynamics in the SZ. This is indeed the case in the test particle simulation and the eccentricity forcing due to the ν_5 is readily apparent (see Figure 11). However, this same effect is not obvious as a 'spike' in the embryo eccentricities near 1.1 AU in the SS simulation. Why is this? Does this result imply that the ν_5 is not important to the evolution of the embryos? The essential difference in the dynamical models of the two simulations is the neglect of close encounters in the test particle simulation. Perhaps two-body scattering events frustrate the resonant forcing of embryos by the ν_5? To develop this idea further and to estimate the importance of the ν_5, we calculate the timescale for embryos to diffuse across a secular resonance due to scattering and compare this with the excitation timescale of a secular resonance to identify the effect that it dominant.

To calculate the time it takes to diffuse across a resonance, we must estimate the embryo diffusion rate and the resonance width. To estimate the diffusion rate

distributed in accordance with the density distribution of the disk.

we follow Hayashi et al. (1977), who showed that the RMS change in the semi-major axis of an object in a swarm of like objects during time t is

$$\left\langle (\delta a)^2 \right\rangle = 1.5\, a^2 \left(\frac{v_{rel}}{v_c} \right)^2 \kappa\, \sigma_e v_{rel} t, \tag{7}$$

where κ is the number density of embryos, v_{rel} is the relative velocity of the embryos, and v_c is the local circular velocity. Hayashi et al. call σ_e the *effective cross section* and define it so that $t = 1/\kappa\sigma_e v_{rel}$ is the 2-body relaxation time. The cross section can be expressed as

$$\sigma_e = 6.5\pi a^2 \left(\frac{m}{M_\odot} \right)^2 \left(\frac{v_{rel}}{v_c} \right)^{-4} \ln \Gamma,$$

where

$$\Gamma = \left[\frac{1}{2} \left(\frac{v_{rel}}{v_c} \right)^2 \left(\frac{d}{a} \right) \left(\frac{m}{M_\odot} \right)^{-1} \right]$$

and where m is the embryo mass and d is the inter-particle spacing. The value of $\ln \Gamma$ is about about 10 for our simulations. The value of κ can be approximated by ρ/m, where $\rho \simeq \Sigma/H$ with Σ being the surface mass density of the disk and $H = a(v_{rel}/v_c)$ being its scale height. We can calculate the crossing time, t_x, of the resonance by setting $\sqrt{\langle (\delta a)^2 \rangle}$ to the width of the resonance, Δ_{res}, so that

$$t_x \simeq \frac{1}{30 \ln \Gamma} \left(\frac{\Delta_{res}}{a} \right)^2 \left(\frac{M_\odot}{\Sigma a^2} \right) \left(\frac{m}{M_\odot} \right)^{-1} \left(\frac{v_{rel}}{v_c} \right)^2 \left(\frac{1}{n} \right), \tag{8}$$

which is similar to the viscous spreading timescale of planetary rings (Goldreich & Tremaine 1978).

We estimate the width of a secular resonance using the following method. Far from a secular resonance the maximum eccentricity, e_{max}, that an object can obtain due to forcing by the other planets in the system is generally small and slowly varying with semi-major axis (a). Here the changes in the minimum periapse ($q_{min} = a(1 - e_{max})$) and maximum apoapse distances ($Q_{max} = a(1 + e_{max})$)

with semi-major axis are dominated by changes in semi-major axis rather than by changes in the forced eccentricity and $dq_{min}/da, dQ_{max}/da > 0$. As the semi-major axis of the resonance is approached the amplitude of the forced eccentricity increases and diverges at $a = a_{res}$. Consequently near the resonance changes in q_{min} and Q_{max} with semi-major axis are dominated by changes in the e_{max} rather than by changes in a. As a secular resonance is approached from the interior ($a_- \rightarrow a_{res}$) at some point the minimum periapse distance due to forced motion begins to decrease with increasing semi-major axis (i.e. $dq_{min}/da < 0$). Similarly as the resonance is approached from the exterior ($a_+ \rightarrow a_{res}$) the maximum apoapse distance begins to increase as a decreases. Thus, the resonance strongly affects the eccentricity of an object in the region between the turning points $dq_{min}/da = 0$ interior and $dQ_{max}/da = 0$ exterior to the resonance. Following Ward et al. (1976), we use the distance between these two points as an effective width of the resonance. To determine the location of the secular resonances and their widths in the giant planet systems studied we have computed the secular Laplace-Lagrange solution of each giant planet system studied and identified the secular resonances that are located interior to the giant planets. The forced eccentricity was computed as a function of semi-major axis and widths of the secular resonances (Δ_{res}) were determined using the criteria described above. We find that $\Delta_{res} = 0.08\,\mathrm{AU}$ and $0.2\,\mathrm{AU}$ for the ν_5 and ν_6 secular resonances, respectively.

With these numbers we can calculate t_x using Equation (8). In order to do this, we must use a system where the resonances have not affected the dynamics of the system. Thus, we will adopt for this purpose the state of the NOPL runs at $t = 10^6$ years. For this system, we find that $t_x = 2.3 \times 10^5$ years near ν_6 resonance and $t_x = 4.0 \times 10^5$ years at the ν_5.

Now we must calculate the timescale for exciting eccentricities by the resonance, t_r. In general this timescale is going to be roughly $2\pi/g_j$, however, we have found

that this estimate is not accurate enough for our purposes. Here we evaluate the timescale for exciting eccentricities by a secular resonance using a numerical approach. We define $t_r \equiv e_0/\dot{e}$, where e_0 is some fiducial eccentricity and $\dot{e}$ is the time derivative of the eccentricity. Since we are interested in situations where secular resonances can excite eccentricities larger than the local background eccentricity, we set e_0 to the eccentricity the NOPL runs at $t = 10^6$ years (0.07), as above. We determine $\dot{e}$ through numerical integrations of test particles in the resonances. In particular, we set $\dot{e} = \Delta e/\tau$, where Δe is the maximum change observed in a large number of test particles spread throughout the resonance in a $\tau = 10^6$ year integration. We found that $\dot{e} = 1.7 \times 10^{-6}\,\mathrm{yr}^{-1}$ in the ν_6 and $\dot{e} = 1.5 \times 10^{-7}\,\mathrm{yr}^{-1}$ in the ν_5. From this, we can estimate that $t_r = 4.1 \times 10^4$ years and 4.7×10^5 years for the ν_6 and ν_5, respectively.

We can use t_r and t_x to understand the differences between the behavior of embryos at the ν_5 and ν_6. In the case of the ν_5 $t_r/t_x = 1.2$ and thus the embryos cross the resonance before they can be significantly excited. On the other hand, $t_r/t_x = 0.2$ in the ν_6 giving the resonance plenty of time to excite the eccentricities of the embryos to large values.

However, the fact that we cannot see the effects of the ν_5 on in Figure 11, does not imply that it is not affecting the system. Indeed, the differences between the temporal evolution of $e^\star$ in the NOPL system and the SS system (see Figure 8B) are due to the effects of the ν_5. This conclusion can be shown with the following simple argument.

The angular momentum of an embryo is $L_e = M\sqrt{GM_\odot a(1-e^2)}$. Thus the rate of change of the angular momentum due to an embryo in the ν_5 secular resonance is

$$\dot{L}_e = -M\sqrt{\frac{GM_\odot a}{(1-e^2)}}\dot{e^2}.$$

The total change in angular momentum of the system in time τ is simply $\Delta L =$

$M\,N_{res}\,\dot{L}_e\,\tau$, where N_{res} is the number of embryos in the resonance which is $2\,\pi\,\mu\,a_{res}\,\Delta_{res}$. Here μ is the number surface density of embryos, a_{res} is the location of the resonance and Δ_{res} is the resonance width. Similarly, the total angular momentum of the material in the SZ is

$$L_{SZ} = 2\,\pi\,M\,\mu\,a_{SZ}\,\Delta a_{SZ}\sqrt{GM_{\odot}a(1-e^{\star 2})}.$$

Assuming that $e^{\star}$ is small and taking into account that the center of the SZ (at $1.3\,AU$), is near the location of the ν_5 resonance (at $1.1\,AU$), we can show that the change in the RMS eccentricity in the SZ due to the presence of ν_5 is

$$\Delta(e^{\star 2}) \approx 2\,\frac{\Delta_{res}}{\Delta a_{SZ}}\,\frac{\dot{e^2}}{1-e^{\star 2}}\,\tau. \tag{9}$$

Through examination of the behavior of test particles in the ν_5 resonance, we determined that $\dot{e^2} = 1.1 \times 10^{-8}\,\mathrm{yrs}^{-1}$.

We can now calculate what the e_{rms} in the SS runs should be if the only two things exciting eccentricities are internal scattering between embryos and the ν_5 secular resonance. As discussed earlier, at $\tau = 10^6$ years $e^{\star} = 0.07$ due to internal scattering (see the discussion following Equation 2). From Equation 9, $\Delta(e^2_{rms}) = 3.7 \times 10^{-3}$, which implies that in the SS runs $e^{\star} = 0.09$. Examining the data presented in Figure 11B, we find that $e^{\star} = 0.10$, in good agreement with this prediction.

Thus, we conclude that the difference in $e^{\star}$ between the SS runs and the NOPL runs is due to the presence of the ν_5 secular resonance at 1.1 AU. This resonance causes the SS runs to be slightly more excited than those of the NOPL runs. However, even though the difference in $e^{\star}$ is measurable for the first few tens of millions of years into the simulation, it is not large enough to significantly change the masses and locations of the terrestrial planets inside of ~ 1.5 AU. An examination of Figures 3B and 3C shows that the large terrestrial planets are similar in the two systems.

We now turn our attention to the other giant planet systems, looking for systems where periapse secular resonances play a more important role in the SZ. The only other strong secular resonance that falls in the region covered by the embryos is in System II and is at 2.4 AU. By strong we mean it can significantly affect the orbits of test particles over 10^7 years. There was one other very strong secular resonance in System IV that without the self gravity of the embryos would have been located at 2.4 AU, but moves beyond the embryos if the self gravity of the disk is included. There were no strong periapse secular resonances in the SZ in any of our systems. Indeed, they were all beyond 2 AU.

In our investigations of the behavior of our simulations we found a periapse secular resonance that was unexpected to us, but could play an important role in the formation of terrestrial planets in systems with one giant planet. One of the methods that we used to separate the effects of secular resonances from mean motion resonances was to perform a 10^7 year SyMBA simulation with the embryos and just the inner giant planet of the system. Our justification was that the locations of the mean motion resonances with the innermost giant planet would not be affected by removing the other giant planets, but there would not be secular resonances in the runs with one giant planet. We believed that there would be no secular resonances because the planet would not be significantly precessing, but the embryos would be precessing because of the presence of the giant planet. Thus, there could be no commensurability.

We were surprised to find that in a simulation that consisted of embryos and the inner giant planet of System II, the vast majority embryos with $1.5 \lesssim a \lesssim 2.1$ AU were driven to large eccentricities on timescales less than a million years, while this did not happen in the simulations with all the giant planets. Figure 12 shows the behavior of one of the embryos in this region. Just before the object's eccentricity is excited, the periapse of the particle is precessing in the positive direction. At

roughly 420,000 years its procession rate slows, turns around, and starts to precess in the opposite direction. During this time the particles maximum eccentricity is pumped from ~ 0.2 to ~ 0.6 due to the long-term ($\sim 20,000\,\mathrm{yr}$) alignment between the periapse of the planet and that of the embryo — i.e. due secular resonance with the planet. This is true even though the planet is not precessing.

So, the question naturally arises: What was wrong with our initial argument that secular resonances would not be present in these systems? Recall that this argument was based on the idea that the embryos would precess, but the planet will not. This assumption is true as long as the embryos' orbits are not crossing, in which case the embryos will be precessing with $\dot{\varpi} > 0$ all throughout the disk. As soon as the embryos' orbits begin to intersect, the self-gravity of the embryos will tend to induce the embryos' apse to precess with $\dot{\varpi} < 0$ (Ward 1981). This occurs because as an embryo follows its orbit, the amount of mass interior to its current location changes — more mass when it is at apoapse and less when it is at periapse. This increases its epicylic frequency, which,by itself, will cause the object to regress. However, the effect of the giant planet is to drive apsidal precession ($\dot{\varpi} > 0$). Thus, depending on the mass distribution of the disk, and the mass and the location of the planet, there may be a location within the disk where these two effects cancel and embryos will not precess. At these locations there will be a secular periapse resonance.

Periapse secular resonances are not the only secular resonances that have played an important role in the eccentricity excitation of our systems. Indeed the secular interaction that played the most important role in System IV (Figure 8E) was a coupling between a nodal (or vertical) resonance (which drives up inclinations) and the Kozai resonance (which couples e and i Kozai 1962).

The behavior of an embryo involved in this coupling is shown in Figure 13. Initially, the embryo is in a nodal or vertical secular resonance with one of the

nodal frequencies of the giant planets. This is shown by the oscillatory behavior of the purple curve in Figure 13 which is the difference between the longitude of the ascending node of the embryo and that of the inner giant planet (for comparison Ω precesses with a period of $72,000$ years). This difference is roughly the critical argument of the nodal resonance. The resonance immediately starts to drive up the inclination of the embryo and by $\sim 27,000$ years it has $i = 20°$. Notice that this resonance does not affect the eccentricity, as the theory predicts.

However, after $\sim 50,000$ years the eccentricity of the embryo begins to change. This is due to the Kozai resonance (Kozai 1962) which is a commensurability between the precession of the longitude of periastron and the precession of the longitude of the ascending node. Thus, in the Kozai resonance the argument of perihelion, ω, librates. The Kozai resonance only occurs for objects with large inclinations. Thus, the nodal resonance make the Kozai accessible by driving up inclinations. The transition into the Kozai occurs at inclinations of i_k, which is a function of the ratio between the semi-major axes of the embryo and the planet. In this problem this ratio is 0.47 and thus according to Kozai (1962) $i_k = 33.2°$. For our embryo, ω starts to librate when the $i = 28°$, which is in relatively good agreement with the theory. This can be observed to happen at $\sim 50,000$ years (green curve).

The Kozai resonance couples the inclination and eccentricity while keeping the angular momentum of the embryo in the direction perpendicular to the invariable plane, L_z, constant. The bottom panel in Figure 13 shows L_z as a function of time. The nearly smooth decrease in L_z for the first 2×10^5 years is due to the nodal secular resonances. Initially the changes in L_z are going into changing i. However, once the embryo is driven into the Kozai resonance by the nodal resonance, the inclination stops growing and the eccentricity starts to grow. Note the rate of change in L_z is constant and thus is unaffected by this. However, until 1.2×10^5 years all the angular

momentum is going into eccentricities. Thus, the Kozai resonance is coupling the the changes in L_z due to the nodal secular resonance to changes in eccentricity. For times later than 1.2×10^5 years, increases in eccentricity are correlated with decreases in inclination as expected by Kozai's theory.

This mechanism is very important in System IV. It drives all particles initially with $2 < a < 2.3\,AU$ to large inclination and eccentricities in only a few tens of thousands of years and keeps them there for millions of years, see Figure 14. This represents $\sim 17\%$ of the mass of the embryos. Another way of thinking about this is that this mechanism pulls about 5% of the total angular momentum out of the system is a very short time. This mechanism is also responsible for driving some of the embryos into the Sun and significantly exciting the eccentricities of the SZ embryos via a process that we call *secular conduction*. We discuss this process in more detail below.

Secular conduction within the embryo disk: As can be seen in Figure 8E, the embryos in the SZ of the System IV runs have significantly higher eccentricities than those in the NOPL runs. Indeed, the $e^\star$ in these runs are the largest of any system besides the one with a Jupiter-mass object on a very eccentric orbit. As we will now argue, objects that are in nodal/Kozai secular resonance at $\sim 2.2\,\mathrm{AU}$ in this system are dynamically exciting embryos in the SZ.

The nodal/Kozai secular resonance excites embryos at $\sim 2.2\,\mathrm{AU}$ onto orbits that cross into the SZ. Figure 14 shows the eccentricity of embryos in one of the System IV runs at 2 million years. The effects of the nodal/Kozai resonance can be seen as large eccentricities between 2 and $\sim 2.4\,\mathrm{AU}$. These objects are crossing the orbits of the embryos in the SZ.

To investigate how the excited embryos affect those in the SZ, we performed the following experiment. We generated two separate populations from the embryos in Figure 14. The first set were those objects in the SZ and the second were those with

semi-major axes between 1.9 and 2.5 AU. We performed a 5×10^6 year integration of just these two sets embryos, without the giant planets or the embryos outside these two regions. Physical collisions were disabled in this simulation. In addition, we did not allow the embryos in the SZ to gravitationally interact with each other. So, the SZ embryos only gravitationally felt the presence of the embryos between 1.9 and 2.5 AU. No other effects were included.

The green curve in Figure 15A (marked 'Embryo Sub-population') shows the temporal behavior of $e^\star$ in this simulation. Also shown for comparison are $e^\star$ in the full-up System IV runs in black and $e^\star$ in the NOPL runs in orange, which are the same data that are shown in Figure 8E. There is excellent agreement between this test simulation and that for the full-up System IV runs, demonstrating that it is indeed the objects in the nodal/Kozai secular resonance that are responsible for exciting the SZ embryos.

The next question to ask is what dynamical mechanism couples these two populations. The natural first guess is that it is gravitational scatterings between embryos. From Hayashi et al. (1977), the RMS change in the semi-major axis and eccentricity of an object in a swarm that is interacting with a different population during time t is:

$$\left\langle (\delta a)^2 \right\rangle = 0.69\, n\, \sigma_e\, a^2\, t\, v_{rel}\, \left\langle e^2 \right\rangle , \tag{10}$$

$$\left\langle (\delta e)^2 \right\rangle = 0.43\, n\, \sigma_e\, t\, v_{rel}\, \left\langle e^2 \right\rangle ,$$

where the symbols have the same meaning as in Equation (7) except that v_{rel} is the relative velocity of the two populations and $\left\langle e^2 \right\rangle$ refers to the swarm.

We can now calculate the expected changes due to scattering in the SZ between 2×10^6 and 4×10^6 years. Using the appropriate values for this situation, we find that Equation(10) predicts that $(\delta a)_{RMS} = 8.2 \times 10^{-4}$ AU and $(\delta e)_{RMS} = 5.4 \times 10^{-4}$. In our simulations, however, we find $(\delta a)_{RMS} = 9 \times 10^{-4}$ AU and $(\delta e)_{RMS} = 0.08$. The fact that the theory predicts the change in semi-major axis quite well, but fails to

produce the correct change in eccentricity by over two orders of magnitude strongly suggests that some other mechanism is to blame for the eccentricity changes. In addition, this mechanism must not affect semi-major axes and thus is probably secular in nature.

Indeed, we now show that forced secular motion, as we described above, is the reason for the eccentricity change. We determined this by performing the following numerical experiments where we slightly vary the physical situation to test particular mechanisms. In these types of experiments it is beneficial to minimize the complexity of the system as much as possible. Thus, we replaced the objects in the SZ with massless test particles and held the orbits of the perturbers (i.e. those objects near $\sim 2\,\mathrm{AU}$ that were excited by the nodal/Kozai resonance) fixed to insure that the nature of perturbation does not change over the experiment.

The first experiment in this series was one designed to investigate how the simplifications we employ affect the behavior of the system. Thus, in this experiment the sub-population of embryos were used directly without modifying the initial conditions or the underlying physics. The green curve in Figure 15B is the results for the fully interacting sub-population and is reproduced from Figure 15A. The red curve shows the results of this test particle simulation with the same initial conditions. For roughly the first million years the curves are the same, indicating that these test particle simulations are reasonable facsimiles of the fully interacting runs for this timescale. The divergence after a million years results from feedback due to the response of the perturbers to the embryos in the SZ.

Now that we know that this test particle representation of our system is reasonable, we can start to experiment. Our first experiment is to confirm the results of Equation 10 that two body scattering is not responsible for the eccentricity growth. This experiment starts with the same initial conditions as the first simulation in this series. However, here we only allow the perturbers to attract the

test particles if they are within 1.7 AU of the star. This distance was chosen since it was the maximum heliocentric distance of any of the test particles. In addition, once a year we randomly changed the longitude of the ascending node, argument of perihelion, and mean anomaly of the perturbers[12] so that any possible resonance is removed. As a result, the only physical process included in this simulation is gravitational scattering. The purple curve in Figure 15B shows $e^\star$ of this system. The change in $e^\star$ in the first 2 million years is 10^{-4} in reasonable agreement with the analytic estimates above.

The next experiment is to investigate whether forced motion can explain the temporal evolution of $e^\star$. In this experiment we need to generate a population of perturbers that do not gravitationally scatter with nor resonate with the test particles. Thus we generated a population that has the same number and mass as previous simulations, but the semi-major axes of all the perturbers was set to the average a from the previous simulations (2.1 AU) and the inclinations were set to the average i from the previous simulations (44°). The average eccentricity of the perturbers from the previous simulations was 0.62. If we used this eccentricity the perturbers would cross the plane of the test particles within the SZ so that close encounters would be unavoidable. To avoid close encounters, we set the eccentricity of the perturbers to 0.67 so that their perihelion distance was inside the location of the test particles. In addition, we set the perturbers' argument of perihelion to zero so that they cross the plane when they are at periapse and apoapse. So as the perturbers orbit they: 1) start in the plane at their periapse which is inside the test particles, 2) they are far above the test particles when then cross the SZ on their

[12] Actually we only randomized the phases if the perturber was beyond 1.7 AU and required that the heliocentric distance after randomizing be beyond this. This was to insure that perturbers did not appear or disappear during a close encounter.

way outward, 3) they are in the plane again when they are at apoapse, which is beyond the location of the test particles, and 4) they are below the test particles when then cross the SZ on their way back in. The remaining angles were chosen at random. Finally, once a year we randomly changed the mean anomaly of the perturbers to remove any mean motion resonances.

The blue curve in Figure 15B shows $e^\star$ of this system and is in good agreement with the behavior of the first test particle simulation (red curve). The faster growth in the current simulation (blue curve) is probably due to the fact that the perturbers are on slightly higher eccentricity orbits. Thus, we conclude that the growth in $e^\star$ in this system is due to the secular forcing by the perturbers.

We refer the process where a significant number of embryos on eccentric orbits secularly force other embryos to large eccentricities as *secular conduction*. One question that occurred to us when we discovered this mechanism is whether it requires massive embryos in order to work, or whether a large number of smaller objects could have the same effect. If the later is true, secular conduction could be important at earlier stages of planet formation. To test this, we repeated the test particle simulation above, increasing the number of perturbers from 12 to 48 while keeping their total mass fixed. This new simulation produced the same results as the original. Thus we conclude that for up to perhaps a hundred perturbers secular conduction will function in a manner that is dependent only on the total mass and not how that mass is divided up between embryos. However, we note that we may not be able to extrapolate this conclusion to very large N.

Secular conduction is also responsible for exciting the eccentricities in the System II's SZ (see Figure 8C). In this system, objects exterior to $\sim 2\,\mathrm{AU}$ are excited to large eccentricities primarily by a strong periapse secular resonance. Usually these objects are very short lived because they suffer close encounters with the inner giant planet. However, a few get trapped in mean motion resonances with

the giant planets thereby increasing their dynamical lifetimes. These objects have eccentricities between ~ 0.3 and ~ 0.6 and secularly force the eccentricities in the SZ. Interestingly, only 4 embryos get trapped in the mean motion resonances, three in the 3:1 and one in the 2:1. These are enough, however, to excite the eccentricities in the SZ.

IV. Summary and Conclusions

The dynamical structure of the newly discovered planetary systems was not expected by most astronomers. Although currently limited to gas giant planets, technologies, like the *Terrestrial Planet Finder* or *TPF*, are in development that may soon allow us to observe terrestrial planets around other stars. Thus, we believe it is time to examine terrestrial planet formation in other planetary systems. Here we studied the role that giant planets play in determining the number, mass, and location of terrestrial planets.

We performed simulations of terrestrial planet formation around solar-mass stars with proto-terrestrial disks similar to what we believe existed in the Solar System using a general model that can account for the formation of the terrestrial planets in the Solar System. The only variable in these simulations (besides stochastic events) was the structure of the giant planet system. In particular, we studied the growth of terrestrial planets in 6 different outer planetary systems: I) no giant planets at all, II) the Solar System's outer planets (SS), III) a system with larger planets than the Solar System, IV) a system with 7 Uranus-mass planets, V) a system with three Saturn-mass objects on eccentric orbits, and VI) a system with a single Jupiter-mass object on a very eccentric orbit. All but the first two systems were taken from our synthetic giant planet systems (Levison et al. 1998) and are shown in Figure 1 and listed in Table 1. For each of these systems, we performed 4 runs in order to start to develop a basic understanding of the dynamical role that giant planets play in terrestrial planet formation. The final planets produced in our simulations can be found in Figure 3.

Every one of our giant planet systems produced at least one planet in the HZ that is massive enough to support plate tectonics through radiogenic heating ($\gtrsim 0.23\, M_\oplus$, see Williams et al. 1997). However, the fraction of runs in each giant planet system that produce such a planet did vary significantly. System NOPL and

System SS basically always produced such a planet. However, Systems II, IV, and V only produced such a system 25% (one in four) of the time. Thus, the giant planets do indeed affect the chances of finding a large planet in the HZ.

In these simulations we find an interesting correlation between the number, mass, and the location of the terrestrial planets. The larger the terrestrial planets, the fewer of them there are, and the closer they are to the central star. If a very large ($\sim 2M_{\oplus}$) object formed, it usually formed alone and it always had a semi-major axis within 0.8 AU of the star.

We show that these relationships are due to dynamical excitation of the embryos' eccentricities by the giant planets. In particular, there is a relationship between the RMS eccentricity in the so called *Study Zone*, between $0.9 < a < 1.5$ AU, and the structure of the terrestrial planets. If the eccentricities become large, objects in the SZ will cross into regions close to the star and tend to collide with embryos there. Thus, the planets interior to the SZ are larger while smaller or no planets form in the SZ. In extreme cases like that of System V, this dynamical excitation drives embryos into the star and thus only small low-mass terrestrial planets form.

Each of the giant planet systems affects the embryos in its unique way. We summarize this in what follows:

System SS: Besides self-stirring, the embryos in the SZ are primarily excited by being scattered into and out of the ν_5 secular resonance. However, this effect is relatively weak and does not significantly effect the terrestrial planets. Thus, the number, sizes, and location of the terrestrial planets within ~ 1.5 AU that formed in the SS runs are similar to those of the runs with no giant planets. These results are consistent with the overall similarities of the results between the Chambers & Wetherill (1998) and Agnor et al. (1999) investigations where the former included giant planets and the latter did not.

System II: The embryos in the SZ are excited by a combination of effects. Objects exterior to $\sim$ 2 AU are excited to large eccentricities primarily by a strong periapse secular resonance. A few of these objects get trapped in mean motion resonances with the giant planets thereby increasing their dynamical lifetimes. These objects then secularly force the eccentricities in the SZ. Thus, dynamical excitation of the embryos by the giant planets in regions other than the SZ can be transferred into the SZ on short timescales via what we call *secular conduction*.

System III: The embryos in the SZ are primarily excited by secular forcing from the inner giant planet.

System IV: The SZ embryos are again excited via secular conduction from the region near 2 AU. These more distant embryos first are trapped in a nodal secular resonance which pumps their inclinations to large values. Once their inclinations reach $\sim 28^\circ$, they enter the Kozai resonance (Kozai 1962), which couples inclinations and eccentricities. Thus, the eccentricities of these embryos grow to large values. Indeed, this combination of resonances can excite the embryos to inclinations approaching 90° and eccentricities on the order of 0.9.

System V: The embryos in the SZ are excited by secular forcing from the giant planet. Since the giant planet is massive and on a very eccentric orbit ($e = 0.8$), the embryos are excited to very large eccentricities.

As can be seen from these descriptions, secular effects are the main cause of excitation by the giant planets. Mean motion resonances do not seem to be very important in the systems we studied. In addition, secular interactions between the embryos can be responsible for the transfer of this excitation from one region of the proto-terrestrial disk to another.

We conclude that the giant planets in a system can have a profound effect on the structure and general habitability of the terrestrial planets. Because of the

complex dynamical interactions that we have observed, we may need to determine the exact orbits of the giant planets in order to determine whether or not terrestrial planets will form in the HZ of a particular system. However, since secular forcing from the innermost giant planet can play a dominate role, we should be able to rule out habitable terrestrial planets in some systems by simply (at least compared to finding terrestrial planets) determining the mass and location of inner giant planet. This issue therefore should be considered when determining targets for the TPF. If the TPF can only study a small number of stellar systems, it may be more effective to first have a smaller and less ambitious mission designed to find and characterize giant planets in those systems.

We would like to thank W. Bottke, R. Canup, L. Dones, and M. Duncan, for useful discussions. We are particularly grateful to W. Ward for help in understanding many of the dynamical effects that we have seen. HFL gratefully acknowledges funding from NASA's *Exobiology* program in support of this work. CA thanks NASA's *Graduate Student Research Program* for generous support.

References

Agnor, C. B., Canup, R. M., & Levison, H. F. 1999. *Icarus*, **142**, 219.

Agnor C. B. & Ward W. R. 2002. *Astrophy. J.* **567**, 579.

Bottke, W. F., Nolan, M. C. ,Greenberg, R. & Kolvoord, R.A. 1994. *Icarus* **107**, 255.

Brouwer, D. & Clemence, G.M. 1964. 'Methods of Celestial Mechanics' (Academic press, New York, NY).

Butler, R. P., Marcy, G. W., Fischer, D. A., Vogt, S. S., Tinney, C. G. Jones, H. R. A., Penny, A. J.& Apps, K. 2002. To appear in *Planetary Systems in the Universe: Observations, Formation and Evolution*, eds. A.Penny, P.Artymowicz, A.-M. Lagrange, and S. Russell (San Francisco: ASP).

Chambers, J.E. 1999. *Mon. Not. Roy. Astron. Soc.* **304**, 793

Chambers J. E. 2000. *Earth Moon and Planets* **81**, 3.

Chambers J. E., 2001. *Icarus* **152**, 205.

Chambers J. E. & Wetherill G. W. 1998. *Icarus* **136**, 304.

Duncan, M.J., Levison, H.F.& Lee M.-H. 1998. *Astron. J.*, **116**, 2067.

Goldreich P.& Tremaine S. D., 1978. *Icarus* **34**, 227.

Greenberg R., Hartmann W. K., Chapman C. R.& Wacker J. F., 1978. *Icarus* **35**, 1.

Hayashi C., Nakazawa K.& Adachi I., 1977, *Pub. Astron. Soc. Japan* **29**, 163.

Kasting, J.F., Whitmire, D.P., & Reynolds, R.T. 1993. *Icarus*, **101**, 510.

Kokubo E. & Ida S. 1998. *Icarus* **131**, 171.

Kortenkamp S. J. & Wetherill G. W., 2000. *Icarus* **143**, 60.

Kozai, Y. 1962. *Astron. J.*, **67**, 591.

Levison, H.F. & Duncan, M.J. 2000. *Astron. J.*, **120**, 2117.

Levison, H.F., Lissauer, J.J., & Duncan, M.J. 1998. *Astron. J.* **116**, 1998.

Lissauer, J. J., & Stewart, G. R. 1993. In *Protostars and Planets III*, eds. E. H. Levy and J. I. Lunine eds (Tucson: Univ. of Arizona Press) 1061.

Marcy, G. W., Butler, R. P., Fischer, D., Vogt, S. S., Lissauer, J. J., & Rivera, E. J. 2001. *Astrophy. J.* **556**, 296.

Marcy, G. W., Cochran, W. D., & Mayor, M. 2000. In *Protostars and Planets IV,* eds. V. Mannings, A.P. Boss, and S.S. Russell (Univ. Arizona Press, 2000), 1285.

Mayor, M., Naef, D. Pope, F., Queloz, D., Santos, N. C., Udry, S., & Burnet, M. 2002. To appear in *Planetary Systems in the Universe: Observations, Formation and Evolution*, eds. A.Penny, P.Artymowicz, A.-M. Lagrange, and S. Russell (San Francisco: ASP).

Naef, D., Latham, D.W., Mayor, M., Mazeh, T. Beuzit, J.L., Drukier, G.A., Perrier-Ballet, C., Queloz, D., Silvan, J.P., Torres, G., Udry, S., & Zucker, S. 2001. *Astron. & Astrophy.* **375**, L27.

Öpik, E.J. 1951. *Proc. R. Irish Acad.*, **54A**, 165.

Stepinski T. F. & Black D. C., 2000, *Astron. & Astrophy.* **356**, 903.

Stewart G. R. & Ida S., 2000. *Icarus* **143**, 28.

Tremaine, S. D. 1990. In *Baryonic Dark Matter*, eds. D. Lynden-Bell and G. Gilmore, (Dordrecht: Kluwer) 37.

Ward W. R., 1981. *Icarus* **47**, 234.

Ward W. R., 1993. *Icarus* **106**, 274.

Ward W. R., Colombo G.& Franklin F. A. 1976. *Icarus* **28**, 441.

Weidenschilling, S.& Cuzzi, J. 1993. In *Protostars and Planets III*, eds. E. H. Levy, J. I. Lunine, M. S. Mathews (Tucson: Univ. of Arizona Press.), 1031.

Weidenschilling S. J., Spaute D., Davis D. R., Marzari F.& Ohtsuki K., 1997. *Icarus* **128**, 429.

Wetherill G. W. 1986. In *Origin of the Moon*, eds. W.K. Hartmann, R.J. Phillips, & C.J. Taylor (Houston: LPI) 519.

Wetherill, G. W. 1988. Accumulation of Mercury from Planetesimals, In *Mercury*, eds. F. Vilas, C. Chapman, and M. Matthews (Tucson: Univ. of Arizona Press.), 670.

Wetherill G. W., 1990. *Annual Review of Earth and Planetary Sciences* **18**, 205.

Wetherill, G. W. 1992. *Icarus* **100**, 307.

Wetherill, G. W. 1994a. *Geochim. Cosmochim. Acta.* **58**, 4513.

Wetherill G. W. 1994b. *Astrophysics and Space Science* **212**, 23.

Wetherill G. W. 1996. *Icarus* **119**, 219 .

Wetherill G. W., & Stewart G. R. 1993. *Icarus* **106**, 190.

Williams D. M., Kasting J. F., & Wade R. A. 1997. *Nature* **385**, 234.

Wisdom, J., & Holman, M. 1991. *Astron. J.* **102**, 1528.

Table 1
Giant Planet Systems

System	Planet	Mass ($M_\oplus$)	a (AU)	e	i (Deg)	e_{max}	i_{max} (Deg)	q_{min} (AU)
SS	G1	318	5.2	0.049	0.33	0.062	0.49	4.88
	G2	94	9.6	0.056	0.93	0.090	1.02	8.69
	G3	15	19.2	0.044	1.02	0.078	1.18	17.69
	G4	17	30.1	0.011	0.73	0.023	0.80	29.32
II	G1	746	3.77	0.057	0.02	0.063	0.06	3.54
	G2	1261	6.22	0.015	0.02	0.021	0.05	6.05
	G3	593	11.22	0.012	0.01	0.031	0.05	10.62
	G4	23	24.95	0.048	1.32	0.100	1.40	22.29
	G5	2	39.04	0.054	2.80	0.088	2.87	35.88
III	G1	7	4.08	0.094	0.04	0.153	0.55	3.44
	G2	26	5.38	0.017	0.15	0.081	0.47	4.95
	G3	21	8.13	0.038	0.12	0.058	0.36	7.65
	G4	16	12.64	0.052	0.39	0.075	0.41	11.69
	G5	15	19.01	0.027	0.08	0.057	0.48	17.92
	G6	4	25.97	0.058	0.69	0.121	0.79	22.89
	G7	8	35.41	0.032	0.39	0.066	0.66	33.06
IV	G1	87	4.50	0.162	11.61	0.287	17.80	3.20
	G2	85	7.21	0.109	6.50	0.266	15.19	5.29
	G3	87	21.18	0.101	4.65	0.121	5.11	18.60
V	G1	343	17.37	0.788	21.97	0.788	21.97	3.69

The columns are: 1) planetary system (SS indicates the Solar System), 2) giant planet, 3) planetary mass, 4) semi-major axis (a), 5) initial eccentricity (e), 6) initial inclination (i), 7) larest eccentricity in a 20Myr integration, 8) largest inclination, 9) smallest perihelian distance in a 20Myr integration.

Figure Captions

Figure 1— The giant planet systems used in our simulations. Positions of a circle along abscissa indicates the planet's semi-major axis. The size of the circle indicates the planetary mass (radius $\propto$ mass$^{1/3}$). In addition, the mass of the planet, in $M_\oplus$, is printed above each planet. The markings beneath each planet indicate the range of distances from the central star (periastron and apastron) with the central vertical line indicating the semi-major axis.

Figure 2— Initial conditions for embryos. The top panel shows the initial eccentricity as a function of semi-major axis. The bottom panel shows the initial inclination.

Figure 3— A comparison between the real terrestrial planets in our Solar System and the 24 terrestrial planet systems created during our simulations. The simulated systems are seen at 2×10^8 years. Positions of a circle along abscissa indicates the planet's semi-major axis. The size of the circle indicates the planetary mass (radius $\propto$ mass$^{1/3}$). In addition, the mass of the planet, in $M_\oplus$, is printed above each planet. The markings beneath each planet indicate the range of distances from the central star (periastron and apastron) with the central vertical line indicating the semi-major axis. A) The real terrestrial planets. B) Fictitious terrestrial planets with no giant planets. C) Fictitious terrestrial planets that grew under System SS. D) System II. E) System III. F) System IV. G) System V.

Figure 4— The eccentricity and semi-major axis of planets in one of our System NOPL runs at 2×10^8 years (TOP) and 10^9 years (BOTTOM). The size of the symbol is related to the mass of the planet. The horizontal 'error-bars' indicate the range of distances from the central star (periastron and apastron).

Figure 5— The relationship between the mass of the largest terrestrial planet in a system and the mass weighted average semi-major axis of the terrestrial

planets. To calculate the later value, only terrestrial planets that were not on giant planet-crossing orbits and those that have suffered at least two mergers are used (see text for explanation). Each symbol represents a combination of the 4 runs that we performed under each of the 6 giant planet systems. The 'errors bars' show the range under each giant planet system. The shaded region shows the location of the Habitable Zone.

Figure 6— Similar to Figure 5 except that this figure shows the relationship between the mass weighted average semi-major axis of the terrestrial planets at 2×10^8 years and the RMS eccentricity in the SZ at 10^7 years.

Figure 7— **LEFT:** Top) The eccentricity and semi-major axis of the embryos in one of our System NOPL at 10^7 years. The horizontal 'error-bars' indicate the range of distances from the central star. Bottom) Probability per year that a target body with $a = 1.2\,AU$, $e = 0.15$, $i = 5.7°$, and $M = 0.089 M_\oplus$ will collide with each of its neighbors. **RIGHT:** Same as LEFT but for one of our System II runs and with a target with $a = 1.3\,AU$, $e = 0.24$, $i = 5.5°$, and $M = 0.104 M_\oplus$.

Figure 8— The temporal behavior of $e^\star$ for the embryos in each giant planet system. The curves show the average of the 4 runs in each system. The orange curve is the same in each panel and shows this behavior for the System NOPL runs. The black curve shows these data for the giant planet system as marked in the legend and is as follows: A) NOPL. B) System SS C) System II. D) System III. E) System IV. F) System V.

Figure 9— The red curves show the temporal behavior of $e^\star$ for the embryos in each giant planet system and are reproduced from Figure 8. The green curves show the temporal behavior of a test particle's eccentricity under the gravitational effects of the innermost giant planet. A) System III. B) System V.

Figure 10— The black curves show the temporal behavior of $e^\star$ for the embryos in

each giant planet system and are reproduced from Figure 8. The green curves show the mean orbit crossing velocity from the same simulations. Note the green scales on the left side of the figure. A) System III. B) System V.

Figure 11— Eccentricity verses semi-major axis for objects under the gravitational effect of the giant planets in our Solar System. A) The embryos from one of our System SS runs at 10^6 years. B) Test particles at 10^6 years. In addition to the giant planets, the test particles were embedded in a $4M_\oplus$ disk with the same surface density distribution as the embryos. The ν_5 and ν_6 secular resonances at located ~ 1.1 AU and ~ 2.2 AU, respectively.

Figure 12— The temporal behavior of an object as it passes through the zero procession secular resonance. This object is responding to the Sun and one giant planet, which is not precessing. The top panel shows the evolution of the object's eccentricity while the bottom panel shows its longitude of perihelion, ϖ.

Figure 13— The temporal behavior of an embryo in the coupled nodal, Kozai secular resonance. We plot the eccentricity (blue), inclination (red), argument of perihelion, *omega* (green), critical argument of the nodal resonance, $\Omega - \Omega_{pl}$ (purple), and angular momentum in the direction perpendicular to the IIP (black).

Figure 14— Eccentricity verses semi-major axis for embryos in one of our System IV runs at 2 million years.

Figure 15— The temporal behavior of $e^\star$. A) The orange and black curves are from one of our System IV runs and System NOPL runs, respectively. The green curve is from a simulation of interactive embryos that consists of a subset of the embryos from the System IV run. See the text about how these embryos where chosen. B) The green curve is the same as that in (A). The other curves show the results of a series of simulations where test particles (TPs)

are interacting with embryos on eccentric orbits. Red: Same initial conditions as for the green curve. However here the perturbers cannot respond to the objects in the SZ because the SZ objects are massless test particles. Purple: same as red curve except test particles can only respond to close encounters with the perturbers. Blue: A test particle simulation were close encounters cannot occur and thus only secular effects are important. See test for details.

FIGURE 1

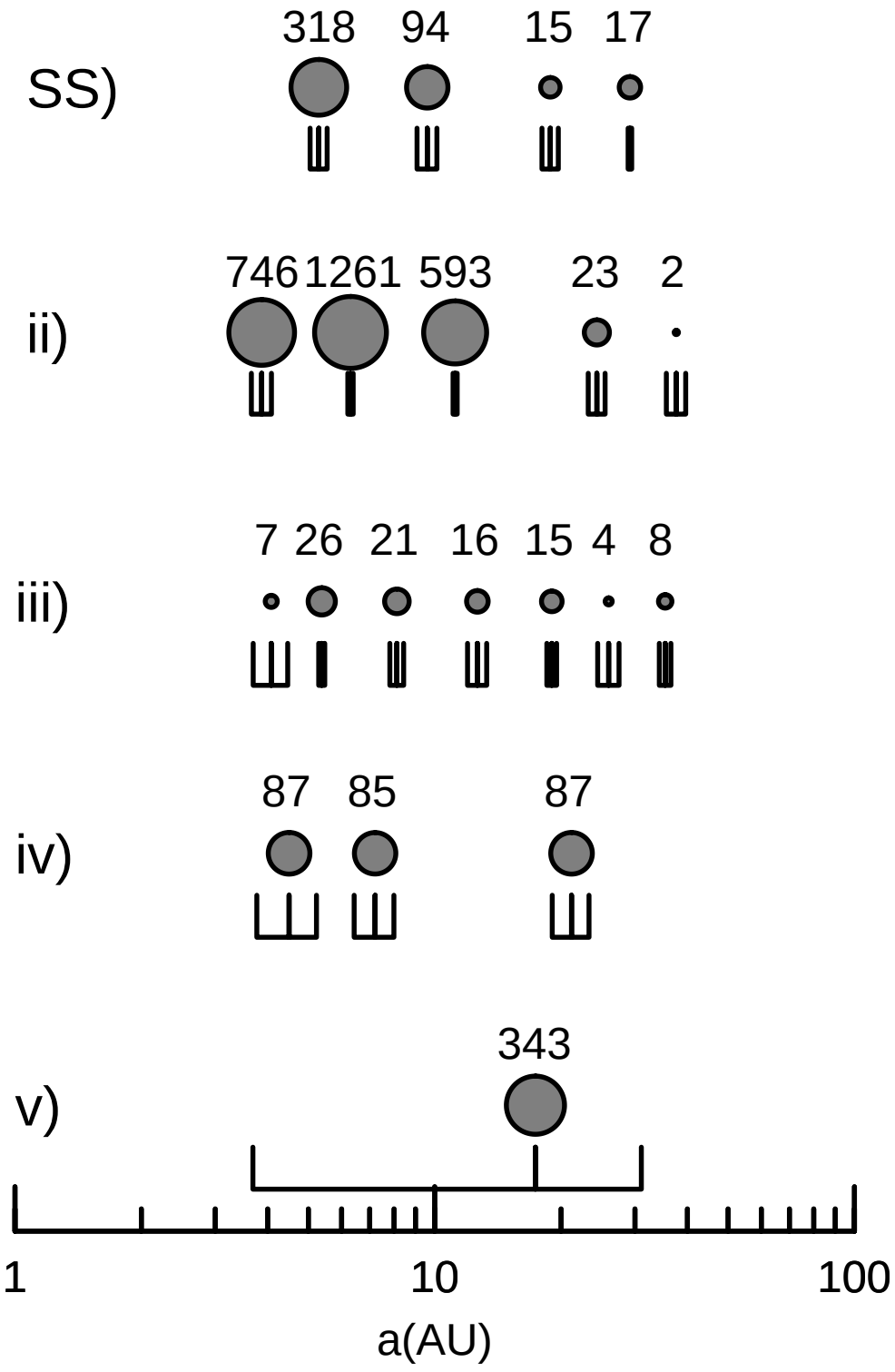
SS)
318
94
15
17
ii)
746
1261
593
23
2
iii)
7
26
21
16
15
4
8
iv)
87
85
87
v)
343
1
10
100
a(AU)

FIGURE 2

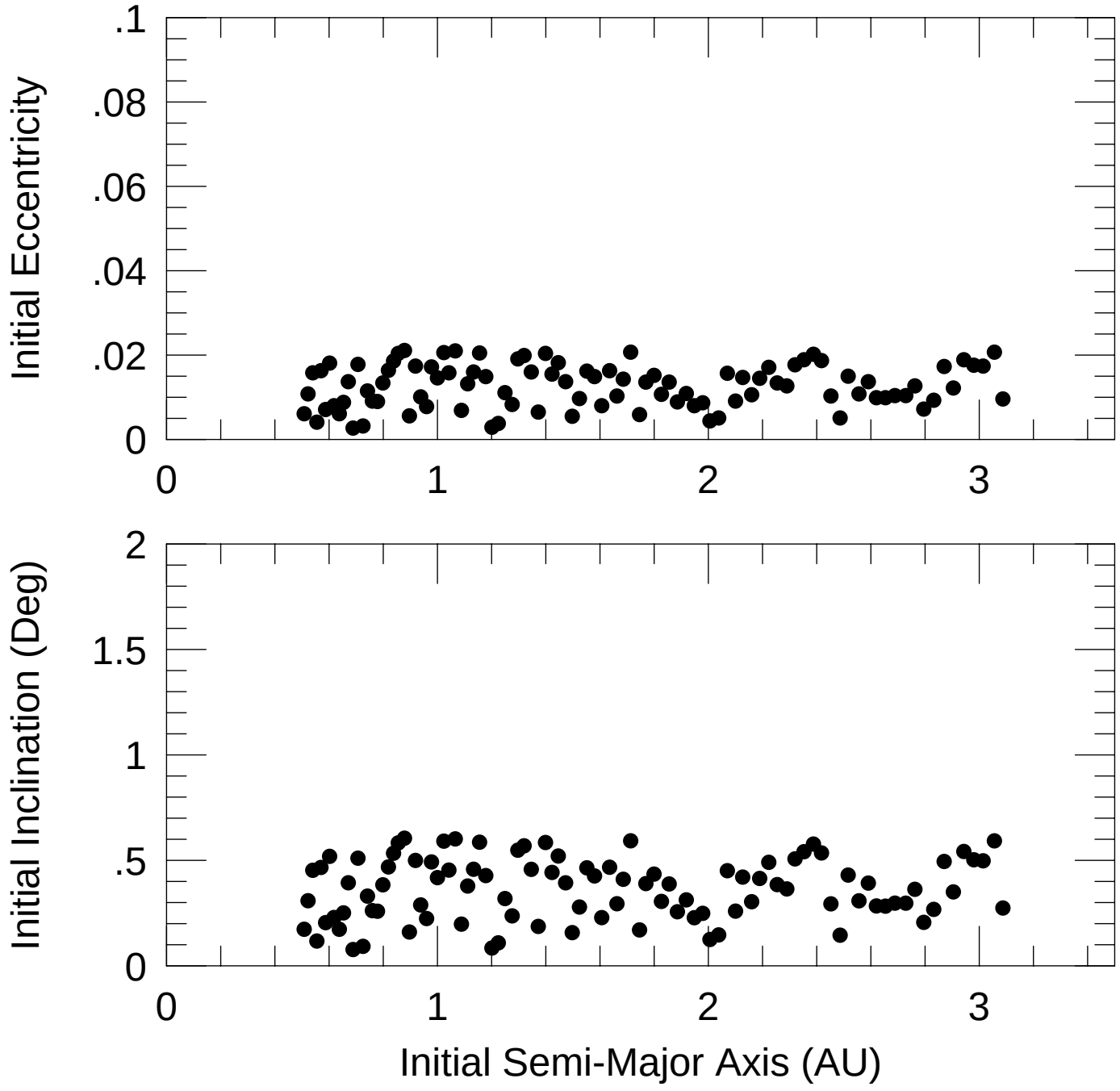
Initial Eccentricity
.1
.08
.06
.04
.02
0
0
1
2
3
Initial Inclination (Deg)
2
1.5
1
.5
0
0
1
2
3
Initial Semi-Major Axis (AU)

FIGURE 3

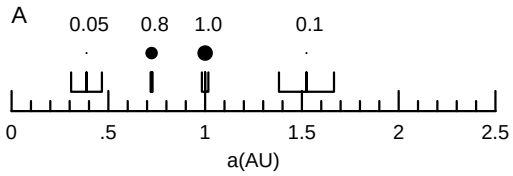
A
0.05
0.8
1.0
0.1
0
.5
1
1.5
2
2.5
a(AU)

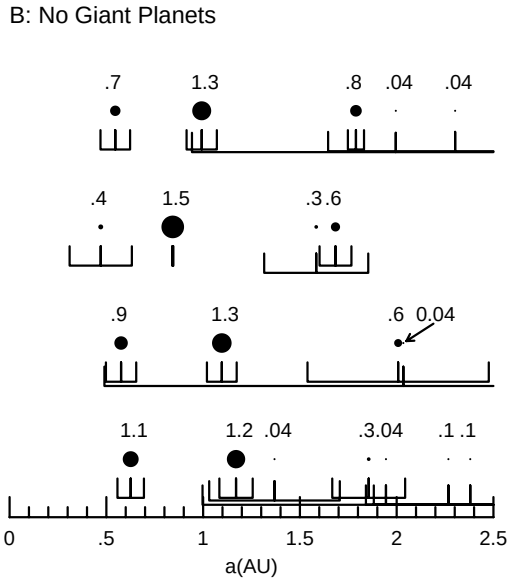
B: No Giant Planets
.7
1.3
.8
.04
.04
.4
1.5
.3
.6
.9
1.3
.6
0.04
1.1
1.2
.04
.3
.04
.1
.1
0
.5
1
1.5
2
2.5
a(AU)

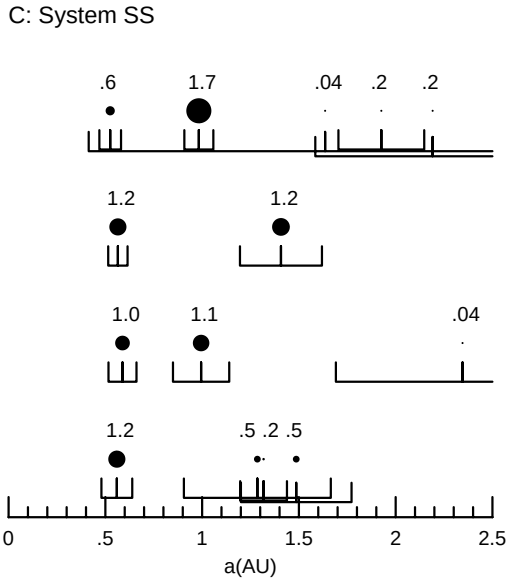
C: System SS
.6
1.7
.04
.2
.2
1.2
1.2
1.0
1.1
.04
1.2
.5
.2
.5
0
.5
1
1.5
2
2.5
a(AU)

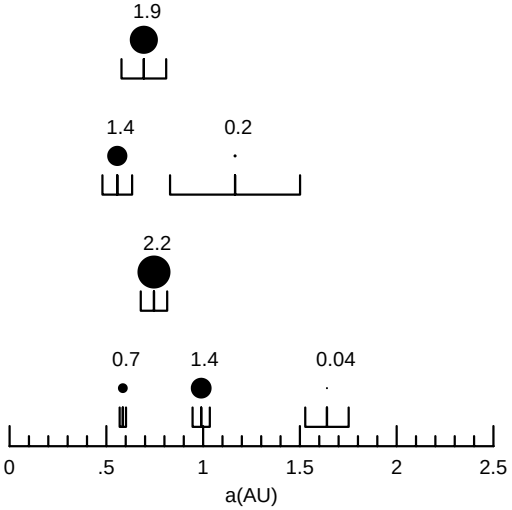
D: System II
1.9
1.4
0.2
2.2
0.7
1.4
0.04
0
.5
1
1.5
2
2.5
a(AU)

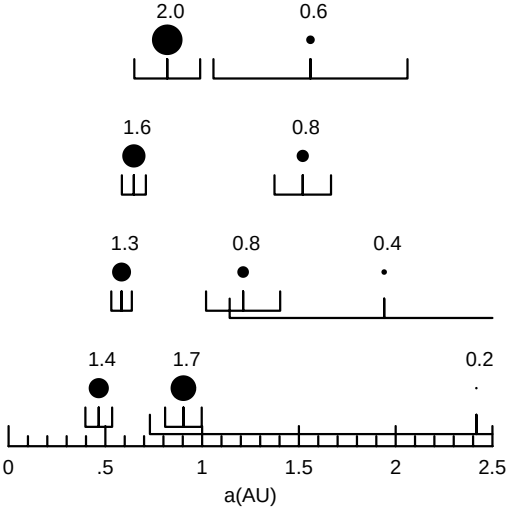
E: System III
2.0
0.6
1.6
0.8
1.3
0.8
0.4
1.4
1.7
0.2
0
.5
1
1.5
2
2.5
a(AU)

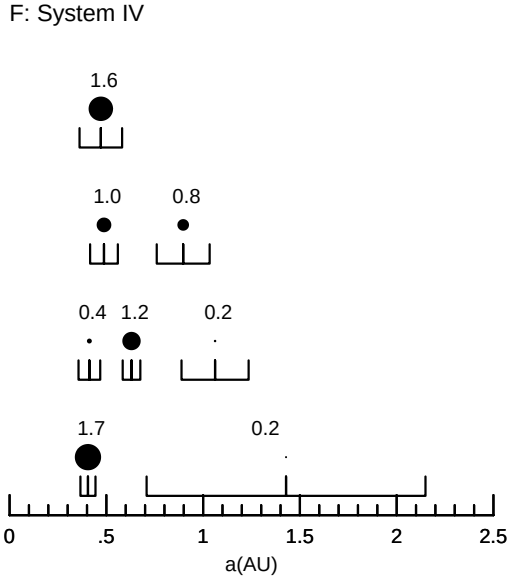
F: System IV
1.6
1.0
0.8
0.4
1.2
0.2
1.7
0.2
0
.5
1
1.5
2
2.5
a(AU)

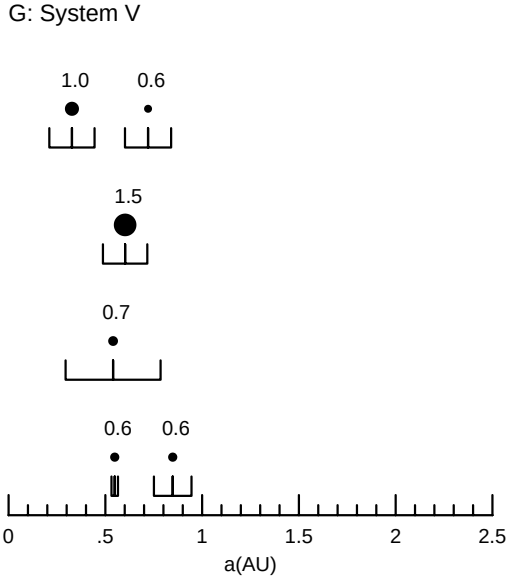
G: System V
1.0
0.6
1.5
0.7
0.6
0.6
0
.5
1
1.5
2
2.5
a(AU)

FIGURE 4

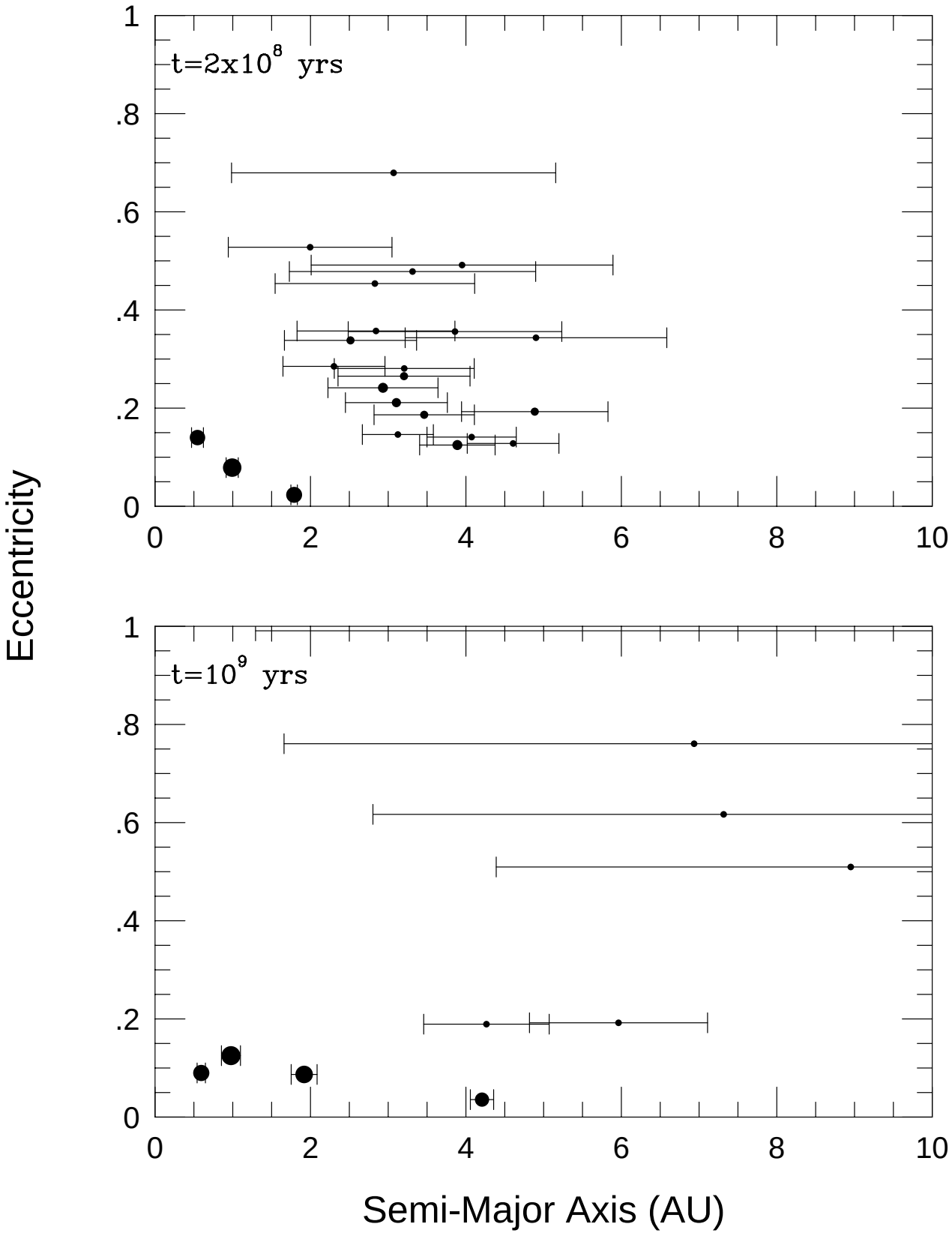
t=2x10^8 yrs
t=10^9 yrs
Eccentricity
Semi-Major Axis (AU)
0
.2
.4
.6
.8
1
0
2
4
6
8
10

FIGURE 5

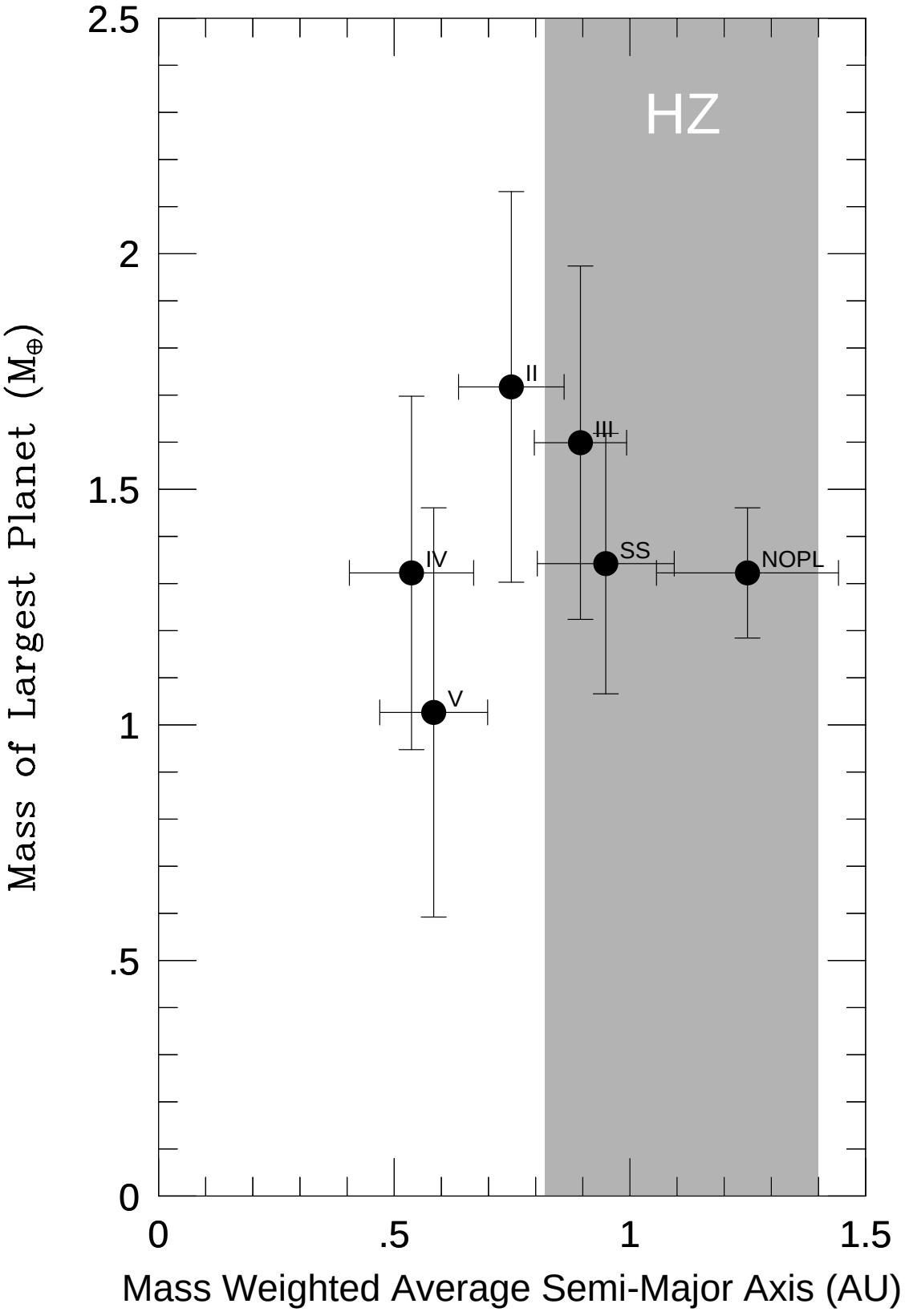
HZ
II
III
IV
SS
NOPL
V
2.5
2
1.5
1
.5
0
0
.5
1
1.5
Mass of Largest Planet ($M_\oplus$)
Mass Weighted Average Semi-Major Axis (AU)

FIGURE 6

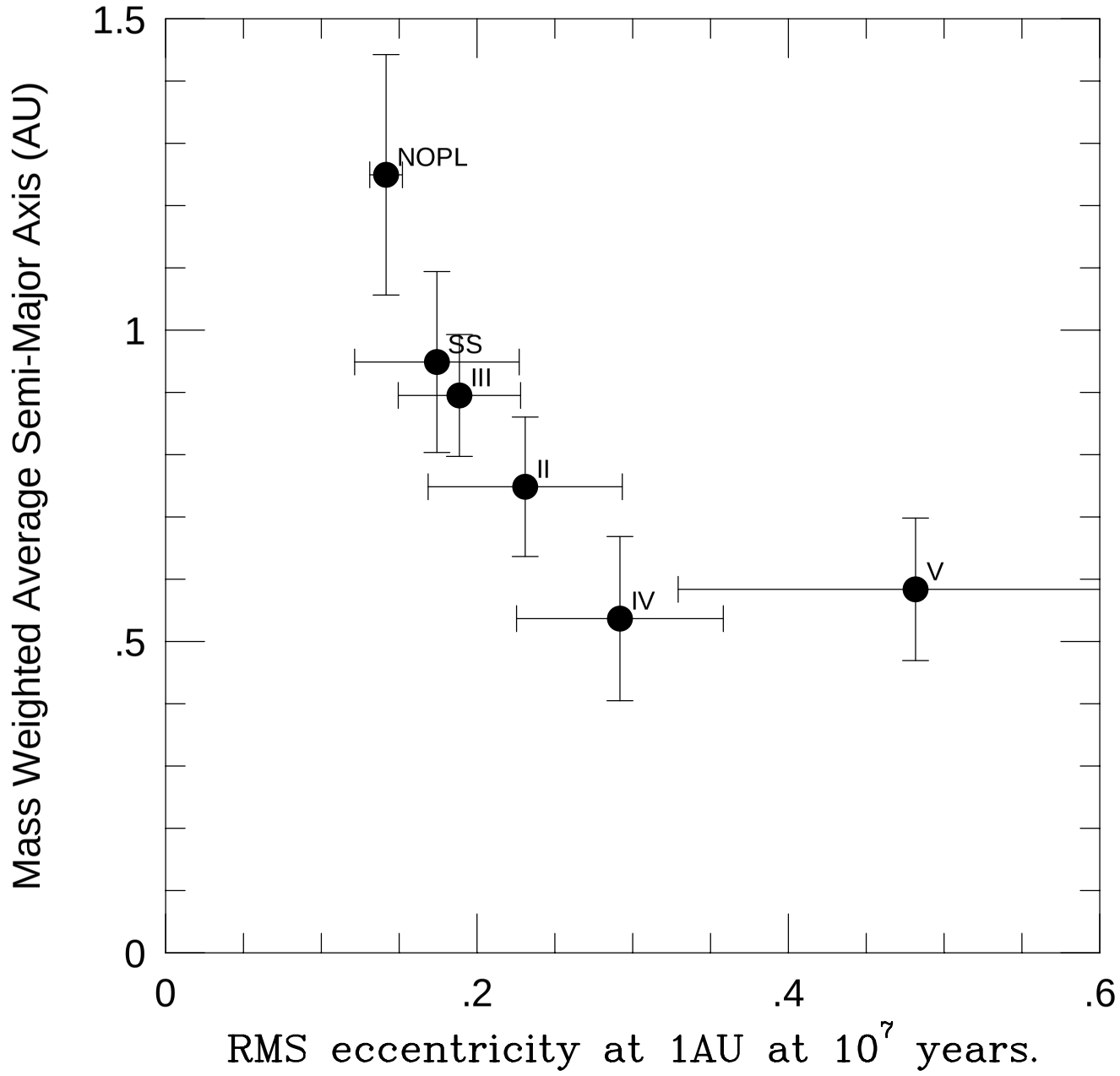
1.5
1
.5
0
0
.2
.4
.6
Mass Weighted Average Semi-Major Axis (AU)
RMS eccentricity at 1AU at 10^7 years.
NOPL
SS
III
II
IV
V

FIGURE 7

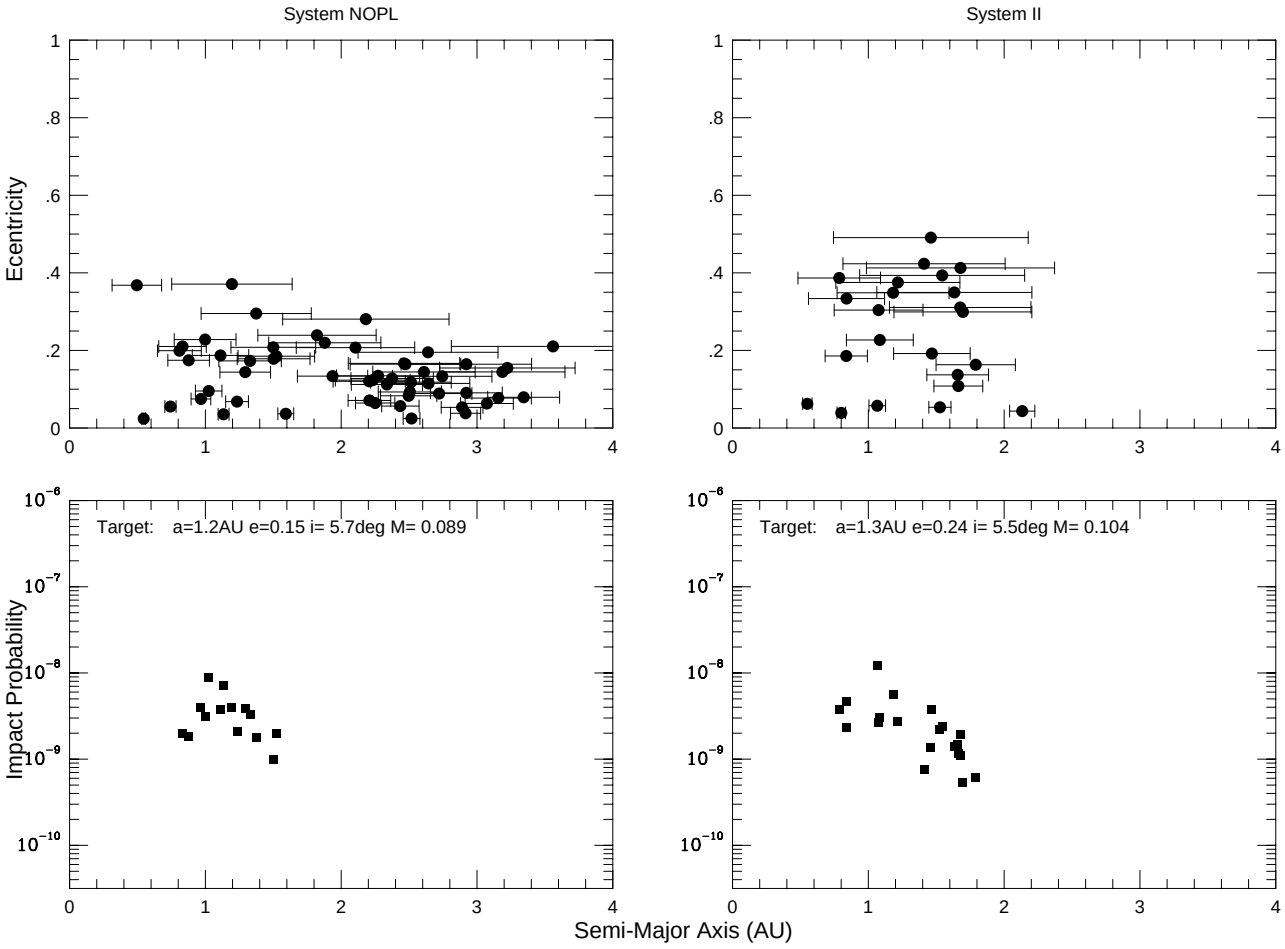
System NOPL
System II
Ecentricity
Impact Probability
Target: a=1.2AU e=0.15 i= 5.7deg M= 0.089
Target: a=1.3AU e=0.24 i= 5.5deg M= 0.104
Semi-Major Axis (AU)

FIGURE 8

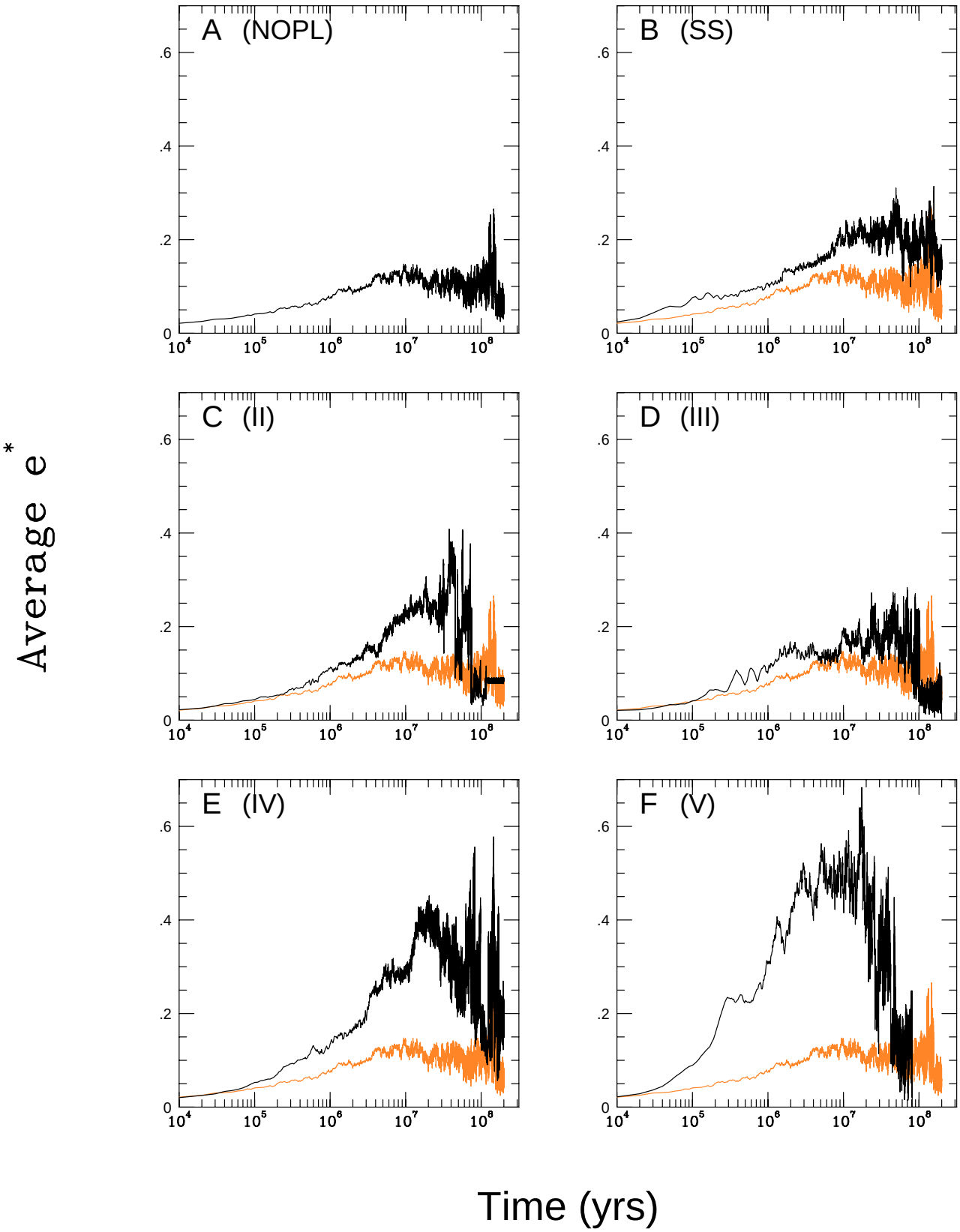

FIGURE 9

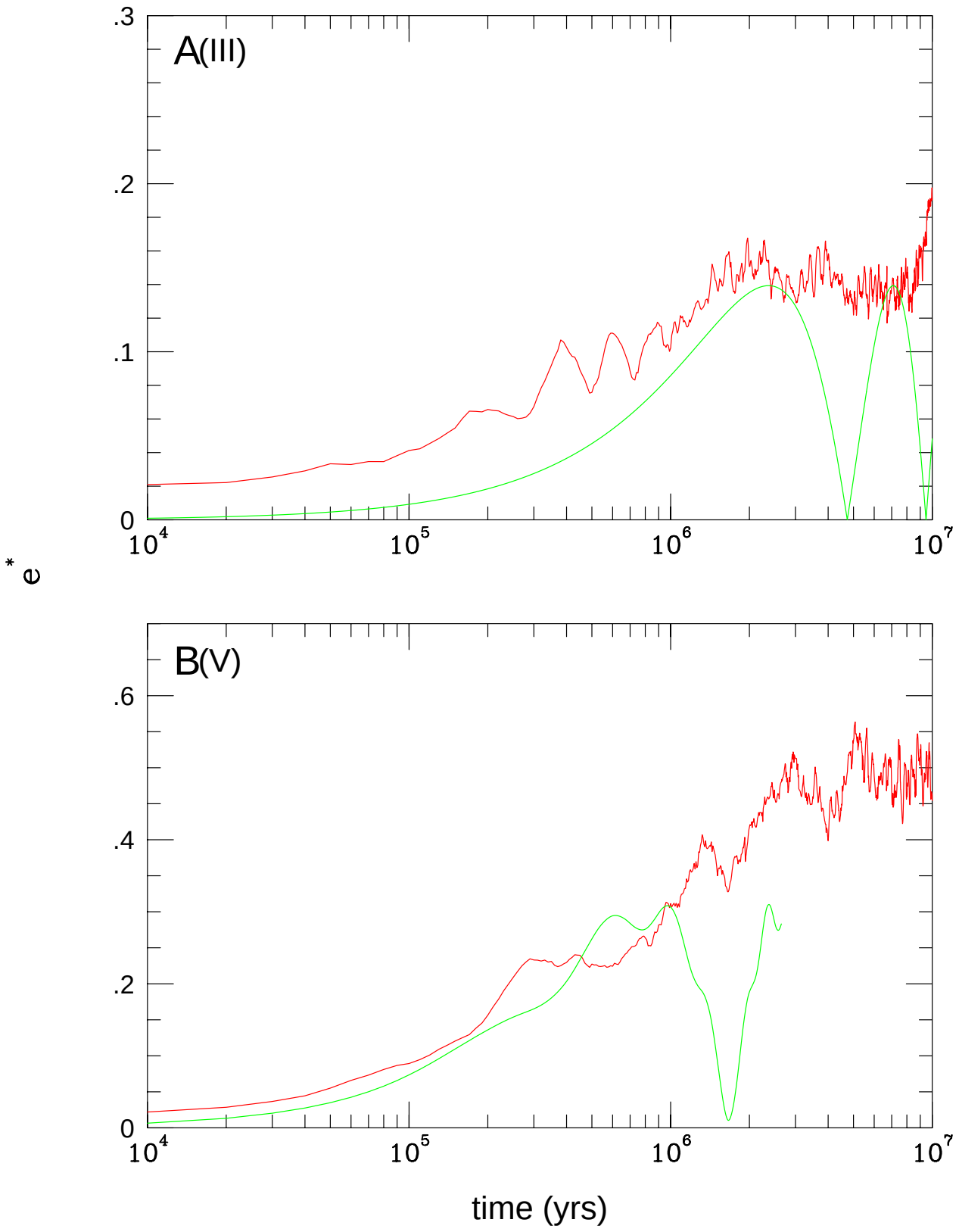

FIGURE 10

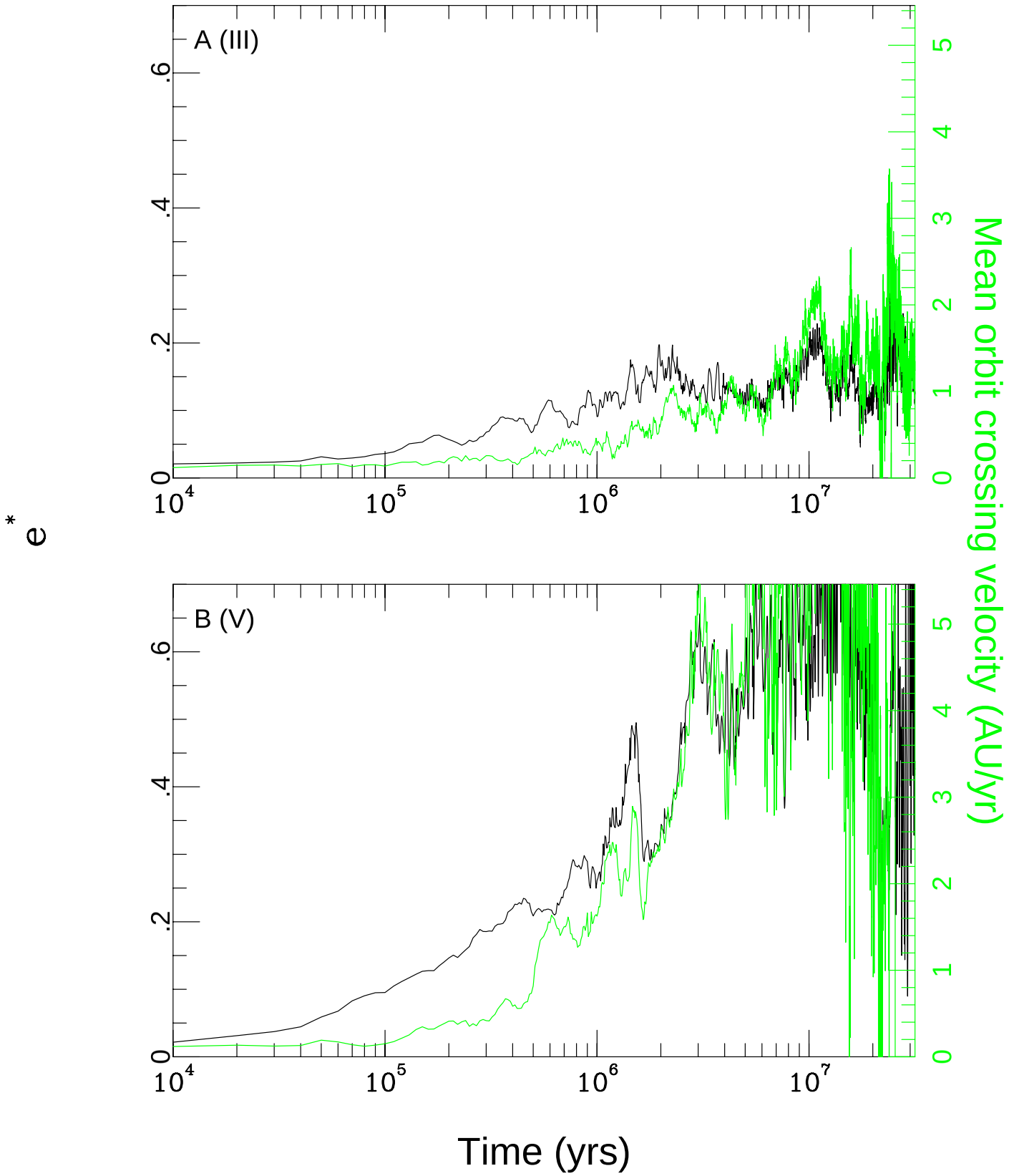
A (III)
B (V)
e*
Mean orbit crossing velocity (AU/yr)
Time (yrs)
0
.2
.4
.6
1
2
3
4
5
10^4
10^5
10^6
10^7

FIGURE 11

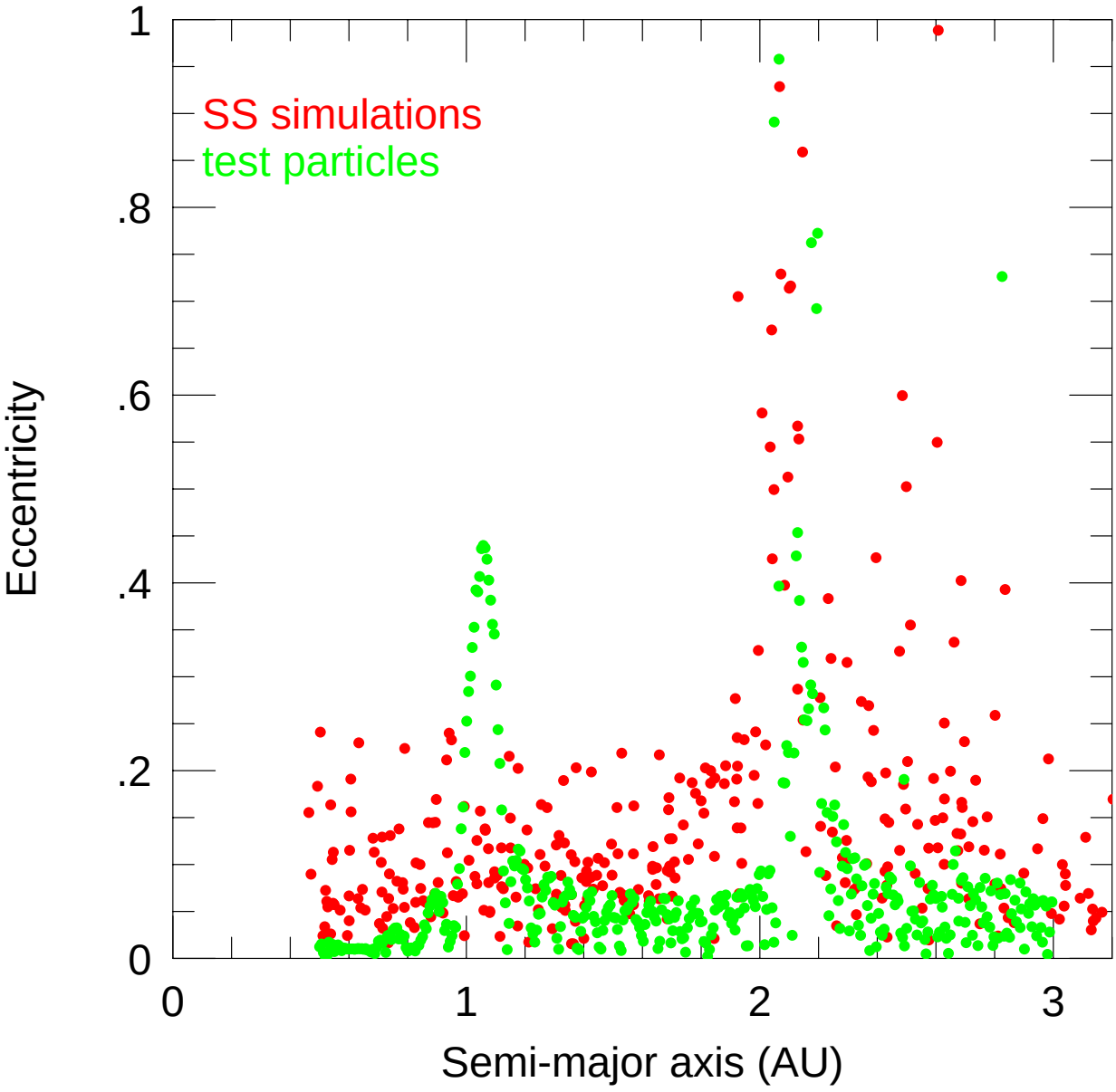
SS simulations
test particles
Eccentricity
Semi-major axis (AU)
0
.2
.4
.6
.8
1
0
1
2
3

FIGURE 12

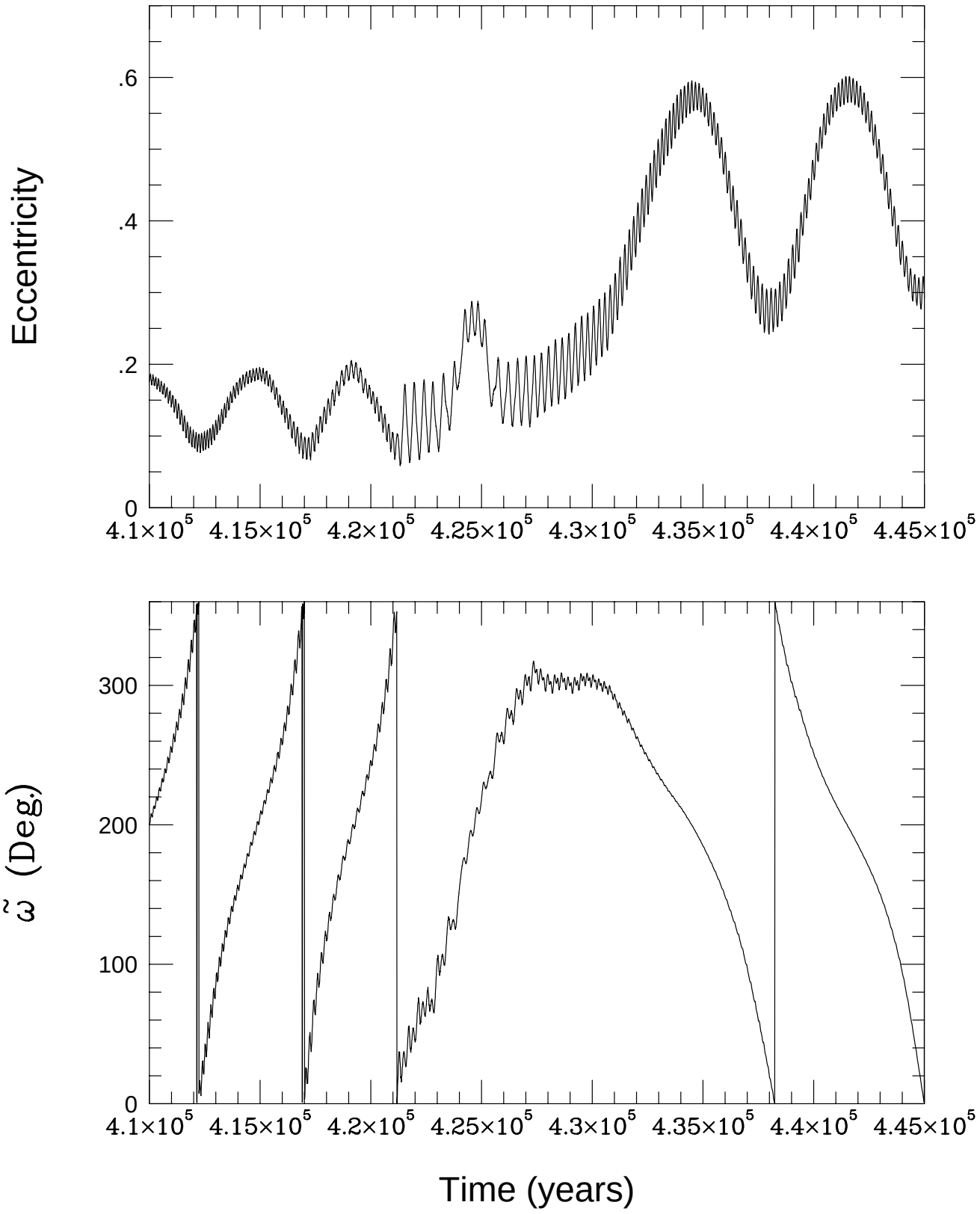
Eccentricity
.6
.4
.2
0
4.1×10^5
4.15×10^5
4.2×10^5
4.25×10^5
4.3×10^5
4.35×10^5
4.4×10^5
4.45×10^5
ω̃ (Deg.)
300
200
100
0
Time (years)

FIGURE 13

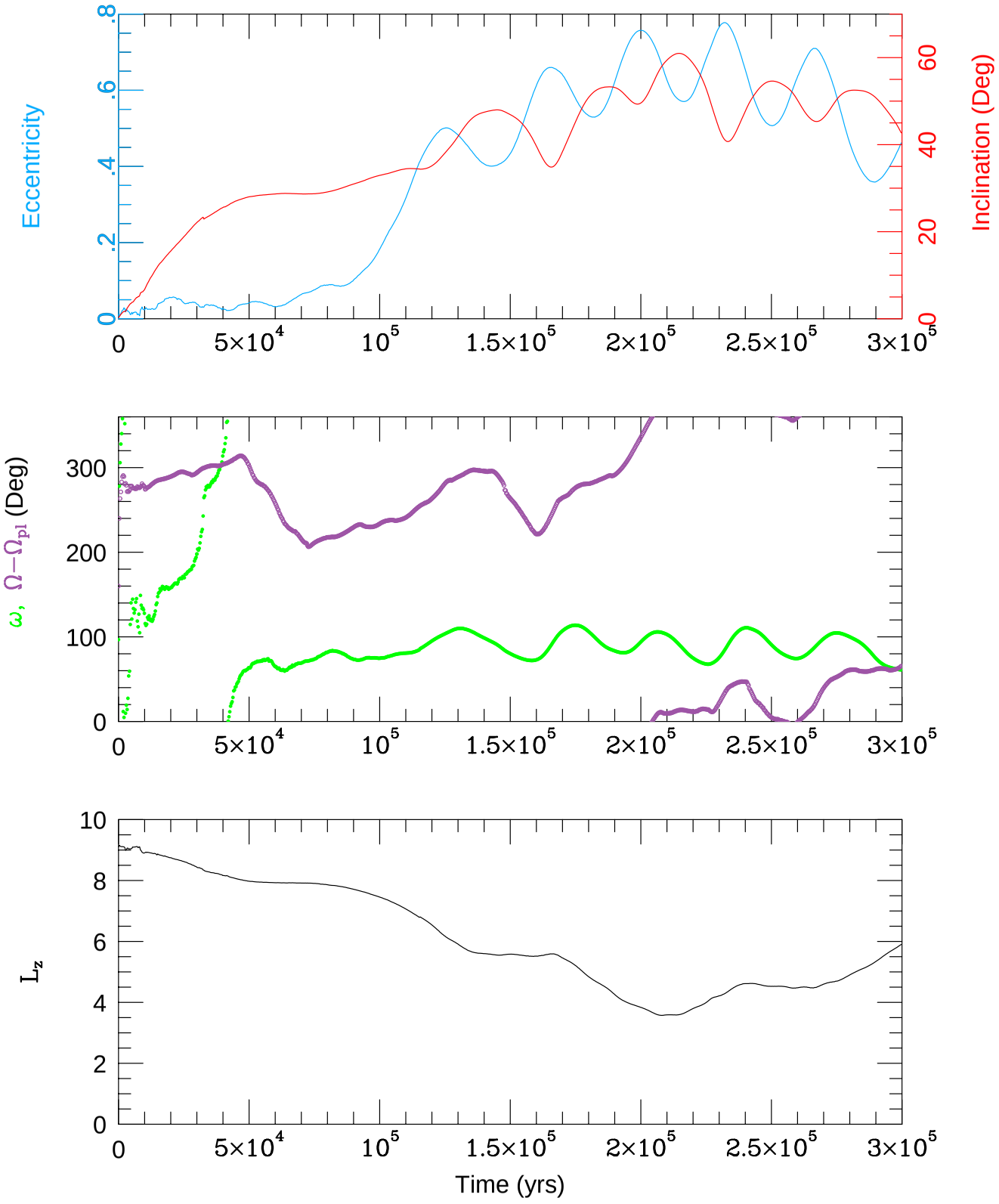
Eccentricity
Inclination (Deg)
0
.2
.4
.6
.8
0
20
40
60
0
5×10^4
10^5
1.5×10^5
2×10^5
2.5×10^5
3×10^5
ω, Ω−Ω_pl (Deg)
0
100
200
300
L_z
0
2
4
6
8
10
Time (yrs)

FIGURE 14

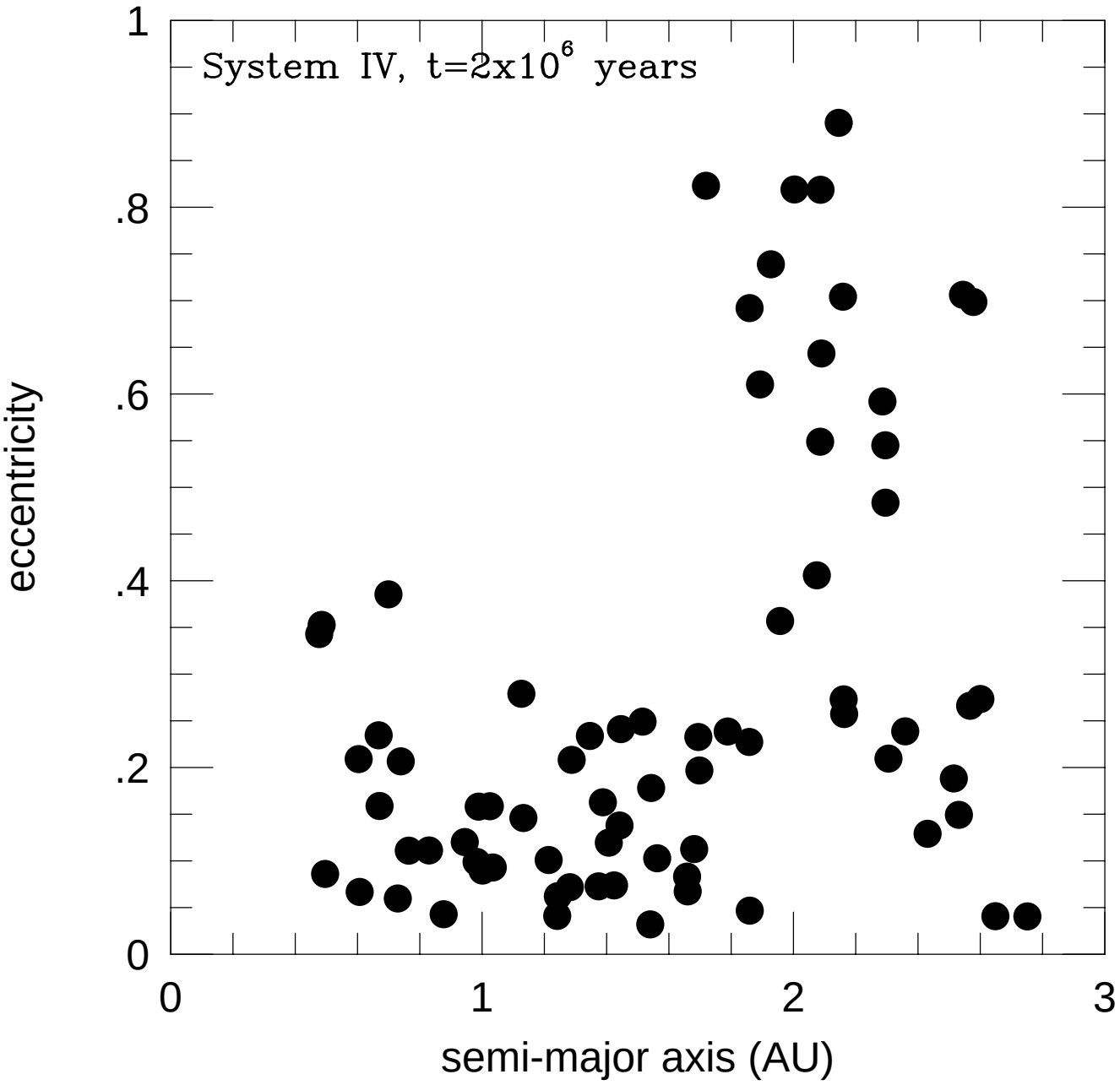
System IV, t=2x10^6 years
eccentricity
semi-major axis (AU)
0
.2
.4
.6
.8
1
0
1
2
3

FIGURE 15

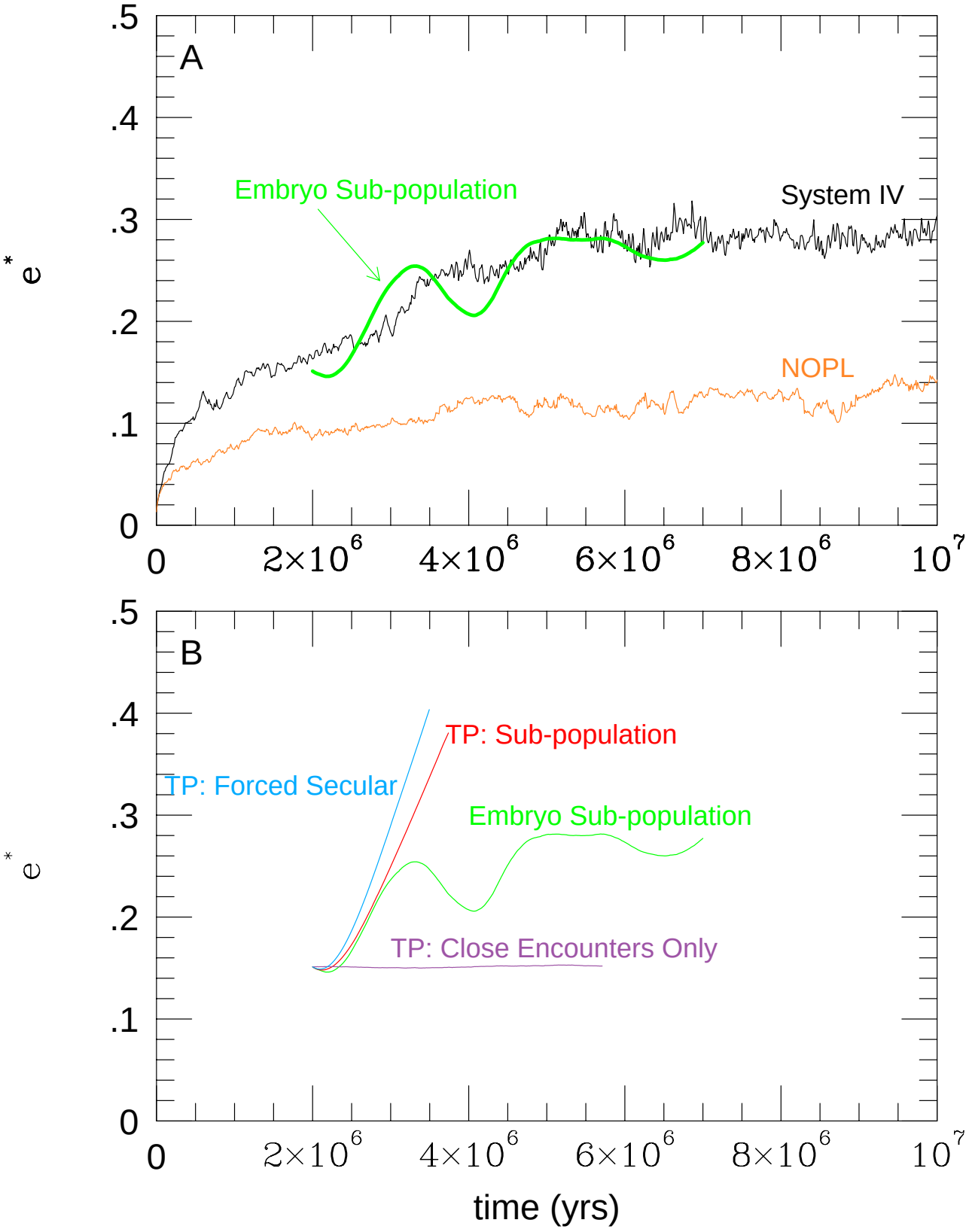
A
B
Embryo Sub-population
System IV
NOPL
TP: Sub-population
TP: Forced Secular
Embryo Sub-population
TP: Close Encounters Only
e*
time (yrs)
0
.1
.2
.3
.4
.5
2×10^6
4×10^6
6×10^6
8×10^6
10^7